JAERI-Research
98-068

HYBRID PARTICLE-IN-CELL(PIC)SIMULATION OF HEAT TRANSFER AND IONIZATION BALANCE IN OVERDENSE PLASMAS IRRADIATED BY SUBPICOSECOND PULSE LASERS

November 1998

Alexei ZHIDKOV and Akira SASAKI

日本原子力研究所
Japan Atomic Energy Research Institute

本レポートは，日本原子力研究所が不定期に公刊している研究報告書です。
入手の問合わせは，日本原子力研究所研究情報部研究情報課（〒319-1195　茨城県那珂郡東海村）あて，お申し越しください。なお，このほかに財団法人原子力弘済会資料センター〒319-1195　茨城県那珂郡東海村日本原子力研究所内）で複写による実費領布をおこなっております。

This report is issued irregularly.
Inquiries about availability of the reports should be addressed to Research Information Division, Department of Intellectual Resources, Japan Atomic Energy Research Institute, Tokai-mura, Naka-gun, Ibaraki-ken 319-1195, Japan.

編集兼発行　日本原子力研究所

JAERI－Research 98－068

Hybrid Particle-In-Cell (PIC) Simulation of Heat Transfer and Ionization Balance in Overdense Plasmas Irradiated by Subpicosecond Pulse Lasers

Alexei ZHIDKOV and Akira SASAKI

Advance Photon Research Center
Kansai Research Establishment
Japan Atomic Energy Research Institute
Mii-minami-machi Neyagawa-shi, Osaka

(Received October 13, 1998)

A 1D hybrid electromagnetic particle-in-cell code with new methods to include particle collisions and atomic kinetics is developed and applied to ultrashort-pulse laser plasma interaction. Using the Langevin equation to calculate the Coulomb collision term, the present code is shown to be fast and stable in calculating the particle motion in the PIC simulation. Furthermore, by noting that the scale length of the change of atomic kinetics is much longer than the Debye radius, we calculate ionization and X-ray emission on kinetics cells, which are determined by averaging plasma parameters such as the electron density and energy over number of PIC cells. The absorption of short-pulse laser by overdense plasmas is calculated in self-consistent manner, including the effect of rapid change of density and temperature caused by instantaneous heating and successive fast ionization of the target material. The calculated results agree well with those obtained from the Fokker-Planck simulation as well as experiments, for non-local heat transport in plasmas with steep temperature gradient, and for the absorption of a short laser pulse by solid density targets. These results demonstrate usefulness of the code and the computational method therein for understanding of physics of short pulse laser plasma interaction experiments, and for application to the gain calculation of short-pulse laser excited X-ray laser as well.

Keywords: Subpicosecond Pulse Laser, Ionization Balance, Heat Flow, Absorption, Simulation, Particle-in-cell, Fokker-Planck Equation, Langevin Equation

ハイブリッドPIC（Particle-In-Cell）シミュレーションコードの開発とサブピコ秒パルスとプラズマの相互作用への応用

日本原子力研究所関西研究所光量子科学センター
Alexei ZHIDKOV・佐々木　明

（1998年10月13日受理）

超短パルスレーザー照射プラズマ中の衝突の効果と原子過程の効果を取り込む新しい手法を用いた1次元PIC（Particle-In-Cell）シミュレーションコードを開発した。PICコードにおける衝突項をランジュバン方程式を用いて計算する方法により、プラズマ中のイオン－電子、電子－電子、イオン－イオンの各衝突過程によるエネルギーと運動量の変化を、モンテカルロ計算に起因する雑音を減らして高速に計算できるようにした。さらに、超短パルスレーザー照射ターゲット内での電子衝突による電離、再結合の効果を、電磁場の計算を行う空間格子の数倍の大きさを持つ原子過程計算用の格子を定義し、平均イオンモデルを用いて計算する方法によって組み込んだ。超短パルスレーザーがターゲットを照射した場合に、急激な加熱によってターゲット物質が電離されることで、温度や電子密度とその時間、空間発展が大きく変化し、それによって吸収係数が変化する効果を取り込んだ計算が行なえるようになった。開発したコードを、急峻な温度勾配を持つプラズマ中の非局所熱伝導、オーバーデンスプラズマへの超短パルスレーザー光の吸収係数の評価に応用した。

計算結果が、以前のFokker-Planckシミュレーションや実験結果と良く一致することを確かめ、今回開発したコードがサブピコ秒レーザーパルスとプラズマの相互作用の物理過程の解明や、そのようなプラズマのX線レーザーへの応用の可能性の評価のために有用であることを明らかにした。

関西研究所：〒572-0019　大阪府寝屋川市三井南町25－1

Contents

目　　次

This is a blank page.

1. INTRODUCTION

Interaction between an ultra short pulse laser and a solid density plasma is interested for various aspects from basic researches such as laboratory astrophysics and high field science, to practical applications including development of X-ray sources and particle accelerators. For example, an overdense plasma irradiated by a subpicosecond laser pulse of moderate intensity ($I=10^{16}$-10^{18} W/cm^2) is considered as an efficient, high brightness table top X-ray source [1-5]. Although the X-ray emission should be well characterized for the optimization for each application, the present experimental diagnostics have limited temporal and spectrum resolution. Therefore, the self-consistent simulation of the laser absorption, heat flow combined with atomic kinetics inside the plasma, which can predict the time dependent X-ray intensity and spectrum, is extremely desirable.

The energy of an ultra short pulse laser is absorbed by the plasma with a steep density gradient through collisional and collisionless processes including the resonance absorption, anomalous skin effect, and vacuum heating (or Brunel mechanism). When an intense laser pulse irradiates the target, high energy electrons are produced from variety of interactions as direct acceleration by the laser electric field or after resonant excitation of plasma waves. In high density plasmas, collisions may dominate the temporal and spatial evolution of the energy distribution of electrons, and their relaxation and transport, that eventually leads to thermalization of electrons and heating of the plasma. The absorption of the ultra short pulse laser is being investigated theoretically in recent years, mainly using particle-in-cell (PIC) method for collisionless plasma [7-13], and using the Fokker-Planck equation in the case collisions are important [14-17]. We develop a PIC code using a rigorous form of the Langevin equation to calculate the effective rate of change of the velocity of the particles due to Coulomb collisions. In contrast to semi-empirical representations of the Langevin equation [18-26] we calculate self-consistently the plasma conductivity including electron-electron collisions. We can compute the conductivity from the case where the heat flow is determined by the Spitzer conductivity to in the case of strong electric field in the plasma. Compared to calculations using the binary collision model (see, for example, [27,28]), our present method is shown to be faster and more stable to calculate the particle motion keeping energy and momentum conserved.

We develop a PIC simulation code with one dimension in space and three dimensions in velocity (1D3V). In addition, using the two wave approximation considering moving frame along the target surface, we successfully model the interaction of oblique incident laser pulses.

The absorption of the laser is also strongly depends on the atomic kinetics inside the plasma. Even in the case of ultra-short pulse laser irradiation, the time required to ionize the target material is shorter than the pulse duration of the laser. Subsequent increase of the electron density and loss of the electron energy by ionization during the laser pulse modify the rate of absorption and the penetration depth of the heat front into the target. We develop a hybrid PIC simulation including the atomic kinetic calculation. We determine a "kinetics" cell by averaging over number of PIC cells to provide good statistics of plasma temperature and density in the cell. Ionization and recombination in the "kinetics" cell are calculated by using the average ion model. The gain and loss of the electron energy is redistributed to the particles as the effective acceleration and deceleration consequently. This variable ionization model allows us to calculate the laser-plasma interaction in more realistic situation from the initially cold, weakly ionized, solid density plasma.

Comparisons of results with those from existing theories and experiments have essential importance to verify accuracy of the method and to demonstrate its advantage over conventional methods. For example, the heat flow in plasmas which have a steep temperature gradient serves a good test case. In the case of heating of a plasma by an intense laser, the scale length of temperature gradient becomes comparable to the electron free path, leading the heat flow to depart from classical value which has a $T_e^{7/2}$ dependence. The non-local heat transport for those cases is so important in laser fusion and other laser-plasma experiments that number of results from the PIC [29] and Fokker-Planck calculation have been published [16,17,38].

More recently, results of detailed measurements of the absorption and X-ray spectrum are reported. In those experiments, high contrast ultra-short pulse lasers are used to drive the target. Results from these experiments are much more reliable and useful for the comparison than earlier ones because the absorption, reflection and heating depend critically on the spatial profile of the plasma produced by prepulse. It is demonstrated in [30] that the plasma reflectivity for the same (τ=120 fs, λ=800 nm, p-polarized) laser pulse changed from 36% to more than 90% with the prepulse delay increased from 4 ps to 18 ps. The main process being responsible to the results is the resonance absorption. Detailed analyses of the process including variable ionization are also important for application of ultra short pulse laser produced plasmas to find out the ways to increase the X-ray brightness.

The paper consist of four parts. In the first part the method employed is described. In the second part the heat flow in a plasma with a steep density gradient is computed. In the third part the heat flow and the ionization balance in a carbon plasma irradiated by a s-polarized pulse is presented. A good agreement of the results with those of the direct solution of the Fokker-Planck-Landau (FPL) equation [15] is shown. In the forth part, the absorption

efficiency of a p-polarized pulse laser and the heat flow into a Si plasma with variable ionization are computed. The results of the efficiency simulation are close to the experimental [30] when the plasma expansion due to laser prepulse is assumed. The strong effect of the elastic collisions and variable ionization on the heat transfer is demonstrated.

2. GENERAL EQUATIONS

Non-ideality and degeneracy of plasma electrons are the main problems in a simulation of the solid-density plasma-laser interaction at moderate laser intensities. These problems arise because initially the plasma is cold. The parameter of ideality,

$$\Gamma_{ei} = e^2(4\pi N_e / 3)^{1/3} / T_e,$$

is equal unity at $T_e=\varepsilon_F$, where the Fermi energy is already about 5-10 eV. At lower temperature, plasma electrons are degenerate and can not be considered as particles. The plasma conductivity may decrease 10^3 times from metal conductivity with temperature increasing from 0.1 eV to 1 eV [31]. To avoid such problems we have to assume that a plasma is heated by a laser prepulse to the temperature when $\Gamma_{ei}<1$ and electrons can be treated like particles, but the temperature is still small enough (10-20 eV,see [14,15]) to simulate the plasma ionization dynamics and the transient X-ray emission .

The self-consistent simulation of a non-degenerate, solid-density plasma should be based on the Fokker-Planck equation with the collisional integral in the Balescu-Lennard form [32,33] which includes effects of plasma polarization,

$$\left[\frac{\partial f_a}{\partial t}\right]_{col} = \frac{\partial}{\partial p_{ai}} \sum_b \int d\mathbf{p}_b w_{ij}^{ab}(\mathbf{v}_a, \mathbf{v}_b)\left(\frac{\partial f_a}{\partial p_{aj}} f_b - \frac{\partial f_b}{\partial p_{bj}} f_a\right), \qquad (1)$$

$$w_{ij}^{ab} = \pi \int \frac{d\mathbf{k}}{(2\pi)^3}\left(\frac{4\pi e_a e_b}{k^2}\right)^2 \frac{k_i k_j \delta(\mathbf{kv}_a - \mathbf{kv}_b)}{|\varepsilon(\mathbf{kv}_a, \mathbf{k})|^2},$$

where $f_a(\mathbf{p}_a)$ is the distribution function of particles "a", $\varepsilon(\mathbf{kv},\mathbf{k})$ is the plasma permitivity. For $\varepsilon=1$ Eq.(1) is the well known Landau collisional integral. To avoid the complexity in the direct calculation of Eq.(1) we also assume that the effect of the permitivity is only in the value of Coulomb logarithm Λ in the FPL equation [34] - the effective collision approximation. Hence the Coulomb logarithm Λ is the parameter of plasma collisionality. Then following the TKN approximation [31] we set $\Lambda_{min}=2$ for an overdense plasma. We

should note that the method of the rigorous Langevin equation allows, in principle, a direct numerical solution of Eq.(1), but such an exact solution is rather expensive.

2.1 LANGEVIN EQUATION. METHOD AND NUMERICAL SCHEME

Coulomb collisions play very important role in the heat and particle transports, and in the ionization balance of a dense, high temperature plasma. There are two approaches to account for such collisions in the PIC simulation. The first (see, for example, [27,28]) is the binary collision (BC) approximation. In spite of its simplicity the BC is very expensive [28] to compute Coulomb collisions of identical particles in a dense plasma. Moreover, the BC can not include the effect of plasma polarization at all. Also there is no proof of conservation of the Maxwellian distribution for a system of identical particles after many collisions. The second approach firstly suggested in [18] is the Langevin equation technique (LET). But equations for electron-electron collisions derived in [18] do not conserve energy and momentum of the system of N electrons even for infinite N. For a real PIC simulation the LET was used in [19] for a low density plasma where electron-atom collisions are important. Now the LET is being developed by a number of authors [20-26]. In [20], the Langevin equation with two dispersion normal random process (a normal process has the Gaussian probability distribution) has been derived and successfully applied for electron runaway simulation by particles. The Spitzer conductivity owned to non-Maxwellian electron-electron collisions has been obtained. The runaway rate is in brilliant agreement with the rate got from solution of the Fokker-Planck equation. The approach of two dispersion normal random process for Langevin equation with Grad approximation for scatterer distribution function both provides the energy and momentum conservation for a system of N identical particles and keeps Maxwellian velocity distribution of particles during self-consistent simulation.

In the frame of the effective collision approximation the PIC plasma simulation, that conforms to the modeling based on the FPL equation, must use the Langevin equation for a motion of charged particles. The equation has the following form,

$$\frac{d\mathbf{p}_k}{dt} = q_k\left[\mathbf{E}(\mathbf{r}_k) + \frac{\mathbf{p}_k}{\gamma_k c}\times\mathbf{H}(\mathbf{r}_k)\right] + \mathbf{P}_k(\mathbf{v}_k), \qquad (2a)$$

where $\mathbf{p}_k$ is the momentum, $\mathbf{r}_k$ is the position , q_k ,M_k are charge and mass of a particle, q_e= -e, q_i=Z_ke, Z_k is the ion charge, **E** and **H** are the electric and magnetic fields.

$$\gamma_k = \sqrt{M_k^2 c^4 + c^2 p_k^2},$$

Here $\mathbf{P}_k(v_k)$ is the collisional term of the equation, including both elastic and inelastic collisions,

$$\mathbf{P}_k(\mathbf{v}_k) = \mathbf{f}_k + (d_k \xi + g_k \eta) \qquad (2b)$$

is the fluctuating acceleration. ξ , η describe the normal random processes with the same characteristics,

$$< \xi_i(t) >= 0; \quad < \xi_i(t)\xi_k(t+\tau) >= \delta_{ik}\delta(\tau), \qquad (2c)$$

$$< \xi_i(t)\eta_k(t+\tau) >= 0, \qquad \int_t^{t+\tau} \xi_k dt' = p_k\sqrt{\tau},$$

where p_k is the normally distributed random number.

To determine functions **f**, d, g in Eq.(2b), Eq.(2a) should be integrated in time [t,t+Δt] with **E=H**=0. A velocity component change due to elastic collisions is

$$\Delta v_i \approx f_i \Delta t + \sum_j [d_{ij}(\mathbf{v} + \aleph \Delta \mathbf{v})\Delta\varphi_j + g_{ij}(\mathbf{v} + \aleph \Delta \mathbf{v})\Delta\psi_j] \approx \qquad (3)$$

$$f_i \Delta t + \sum_j [d_{ij}(\mathbf{v})\Delta\varphi_j + g_{ij}(\mathbf{v})\Delta\psi_j] + \aleph \sum_{j,k} \left(\frac{\partial d_{ij}}{\partial v_k} \Delta v_k \Delta\varphi_j + \frac{\partial g_{ij}}{\partial v_k} \Delta v_k \Delta\psi_j \right),$$

where

$$\int_t^{t+\tau} d_{ij}(\mathbf{v})\xi_j dt = d_{ij}(\mathbf{v} + \aleph \Delta \mathbf{v}) \int_t^{t+\tau} \xi_i dt, \quad \Delta\varphi_i = \int_t^{t+\tau} \xi_i dt, \quad \Delta\psi_i = \int_t^{t+\tau} \eta_i dt.$$

By using Eq.(3) the velocity correlation functions, $<\Delta v_i>$ and $<\Delta v_i \Delta v_j>$, can be calculated. In the limit Δt-0 such correlation functions must give the correlation functions that are determined by elastic cross sections. In the problem under consideration only non-relativistic particle collisions are important. So the representation of the collisional term is given in the non-relativistic form, although the equation can be easily transformed to a relativistic form by using the Budker's collisional integral. In the limit Δt-0 these non-relativistic correlation functions must give the coefficients of the Fokker-Planck

equation, that are expressed by well known Rosenbluth' potentials [34] for a plasma with the Maxwellian ion and electron velocity distributions,

$$A_{i\alpha\beta}(\mathbf{v}) = \lim_{\tau\to 0}\frac{1}{\tau}\left\langle \Delta v_{i\alpha\beta}\right\rangle = N_\beta \int f_\beta(\mathbf{v}_\beta) w_i^{\alpha\beta} d\mathbf{v}_\beta, \qquad (4a)$$

$$B_{ik\alpha\beta}(\mathbf{v}) = \lim_{\tau\to 0}\frac{1}{\tau}\left\langle \Delta v_{i\alpha\beta}\Delta v_{j\alpha\beta}\right\rangle = N_\beta \int f_\beta(\mathbf{v}_\beta) w_{ij}^{\alpha\beta} d\mathbf{v}_\beta,$$

where

$$w_i^{\alpha\beta} = -\left(\frac{\mu_{\alpha\beta}}{M_\alpha}\right)(v_{i\alpha} - v_{i\beta})|\mathbf{v}_\alpha - \mathbf{v}_\beta|\sigma_1(|\mathbf{v}_\alpha - \mathbf{v}_\beta|), \qquad (4b)$$

$$w_i^{\alpha\beta} = \left(\frac{\mu_{\alpha\beta}}{M_\alpha}\right)^2 |\mathbf{v}_\alpha - \mathbf{v}_\beta|^3\left[\delta_{ij}\frac{\sigma_2}{2} + \frac{(v_{i\alpha} - v_{i\beta})(v_{j\alpha} - v_{j\beta})}{|\mathbf{v}_\alpha - \mathbf{v}_\beta|^2}(2\sigma_1 - \frac{3}{2}\sigma_2)\right],$$

are the velocity correlation functions owned to elastic collisions with the transport cross-sections

$$\sigma_1 = \int(1-\cos\theta)d\sigma, \sigma_2 = \int(1-\cos^2\theta)d\sigma.$$

The differential cross-section $d\sigma$ depends on a collisional process. The reduced mass μ_{ab} is determined by usual way.

Then the normalized matrices **f**, d, g can be present in the following form [20]

$$f_i = A_i - \aleph(d_{jk} + g_{jk})\frac{\partial(d_{ik} + g_{ik})}{\partial v_j}, \qquad (5)$$

$$d_{ik} = \frac{1}{\sqrt{2}}(B_+^{1/2})_{ik}, g_{ik} = \frac{1}{\sqrt{2}}(B_-^{1/2})_{ik},$$

where $B_{(-)}^{1/2}$ and $B_{(+)}^{1/2}$ are the roots of the matrix B. The matrix B has only two different real, positive eigenvalues, $\lambda_1 > \lambda_2 > 0$ and thus the roots can be present in the form

$$(B_{\pm}^{1/2})_{ik} = \frac{1}{\sqrt{2\lambda_1} \pm \sqrt{2\lambda_2}}\left(B \pm \sqrt{\lambda_1\lambda_2}E\right), \qquad (6)$$

$$\lambda_{1,2} = a \pm \sqrt{a^3 - ab + c}, \qquad a = (B_{11} + B_{22} + B_{33})/3,$$

$$b = B_{11}B_{22} + B_{11}B_{33} + B_{22}B_{33} - B_{12}^2 - B_{13}^2 - B_{23}^2,$$

$$c = B_{11}B_{22}B_{33} + 2B_{12}B_{13}B_{23} - B_{12}^2B_{33} - B_{13}^2B_{22} - B_{23}^2B_{11},$$

where E is the unity matrix. In a particle simulation

$$B_{ik\alpha\beta}(\mathbf{v}_\alpha, t) = \frac{\Delta v_{x\beta}\Delta v_{y\beta}\Delta v_{z\beta}}{N_\beta}\sum_k w_{ij}(\mathbf{v}_\alpha, \mathbf{v}_\beta^k, t),$$

where $\{\Delta v_x, \Delta v_y, \Delta v_z\}$ is a grid in the velocity space, N_β is the number of β particles, and v_β^k is the velocity of the kth particles.

The parameter $\aleph$ in the Eq. (5) equals zero for collision of the same mass particles (Itoh equation) and equals 1/2 for collisions of light particles with infinite mass particles. Appearance of non zero $\aleph$ in Eq.(5) is a results of transformation of the Itoh equation for the limit M_a/M_b--0. We have to do it analytically because, already at M_a/M_b=0.01, errors of random number calculation affect on results. We should note also that for scattering of light particles by heavy particles the coefficients (4a) do not depend on the distribution function of scatterers. For this case the LET technique and the BC approximation are identical.

By substituting the Coulomb cross-sections

$$\sigma_1(|\mathbf{v} - \mathbf{v}'|) = \frac{1}{2}\sigma_2(|\mathbf{v} - \mathbf{v}'|) = \frac{4\pi e_\alpha^2 e_\beta^2 \Lambda}{\mu_{\alpha\beta}^2 |\mathbf{v} - \mathbf{v}'|^4}$$

into Eq.(5) and by assuming further that the distribution function of scatterers in the e-e collision term has the 8th momentum Grad approximation form

$$f(\mathbf{v}) = \frac{N}{\pi^{3/2} v_T^3}\exp\left(-\frac{(\mathbf{v}-\mathbf{u})^2}{v_T^2}\right)\left[1 - \frac{\mathbf{q}(\mathbf{v}-\mathbf{u})}{v_T^4}\left(1 - \frac{2}{5}\frac{(\mathbf{v}-\mathbf{u})^2}{v_T^2}\right)\right], \qquad (7a)$$

where the thermal velocity v_T and the heat flow $\mathbf{q}$ are

$$v_T^2 = \frac{2}{3} < (\mathbf{v}-\mathbf{u})^2 >, \mathbf{q} = \langle (\mathbf{v}-\mathbf{u})^2 (\mathbf{v}-\mathbf{u}) \rangle,$$

u is the mean velocity, for electron-electron and electron-ion collisional terms we get the equation such that [20]

$$\mathbf{P}_e = -4\pi\Lambda \left(\frac{e^2}{m_e} \right)^2 \left(Z^2 \frac{m_e}{M_i} N_i \frac{\mathbf{v}}{v^3} + \frac{4}{v_{T_e}^2} N_e \frac{\mathbf{w}}{w} G(w) \right.$$

$$\left. - N_e \Phi'(w) \frac{4(\mathbf{qw})}{5v_{T_e}^4} \mathbf{w} \right) + \frac{e^2}{m_e} \sqrt{\frac{4\pi\Lambda Z^2 N_i}{v}} \left(\xi - \frac{\mathbf{v}(\mathbf{v}\xi)}{v^2} \right) \qquad (7b)$$

$$+ \frac{e^2}{m_e} \sqrt{\frac{4\pi\Lambda N_e}{v_{T_e} w}} \left[\sqrt{\Phi(w) - G(w)} \left(\zeta - \frac{\mathbf{w}}{w^2} (\mathbf{w}, \zeta) \right) + \sqrt{2G(w)} \frac{\mathbf{w}}{w^2} (\mathbf{w}, \eta) \right]$$

In Eq.(7) $\mathbf{w}=(\mathbf{v}-\mathbf{u})/v_T$, η, ξ, ζ describe the normal random processes, each of the vectors has three independent components with the mean equals zero and the dispertion equals to $(2)^{-1/2}$.

$$\Phi(w) = 2\int_0^w dx e^{-x^2} / \sqrt{\pi}, \qquad G(w) = [\Phi(w) - w\Phi'(w)] / (2w^2)$$

The plasma parameters are determined on the "kinetics" grid. The process ξ describes plasma electrons scattering by ions, the process ζ describes the moment rotation as a result of electron-electron collision, the process η describes energy redistribution between electrons after the collision, providing the system ergodicity even if there is no electromagnetic field in a plasma. The Eq.(7) conserves the energy of the system of N electrons in contrast to the Monte-Carlo methods that conserve energy of two particles. We should note also that a modification of Eq.(7) for electron- ion collision by including the lowest limit of drift velocity like the Fermi velocity v_F provides the TKN approximation [31] down to few eV for solid-density plasma of Al.

By using the 5th momentum Grad approximation for the ion distribution function (Eq. (7a) with **q**=0) the ion collisional term can be obtained in the following form when electron temperature ,T_e, exceeds the ion temperature, T_i

$$\mathbf{P}_i = -4\pi\Lambda'\left(\frac{(Ze)^2}{M_i}\right)^2 N_i \frac{4}{v_{T_i}^2}\frac{\mathbf{y}}{y}G(y) + \frac{Ze^2}{M_i}\zeta_3\sqrt{\frac{4\pi\Lambda N_e}{v_{T_e}}}\frac{8}{3\sqrt{\pi}}$$

$$+\frac{(Ze)^2}{M_i}\sqrt{\frac{4\pi\Lambda' N_i}{v_{T_i} y}}\left[\sqrt{\Phi(y)-G(y)}\left(\zeta_1 - \frac{\mathbf{y}}{y^2}(\mathbf{y},\zeta_1)\right) + \sqrt{2G(y)}\frac{\mathbf{y}}{y^2}(\mathbf{y},\zeta_2)\right], \qquad (7c)$$

$$\mathbf{y} = (\mathbf{v}_i - \mathbf{u}_i)/v_{T_i}$$

The vectors ζ_1, ζ_2 describe the random processes for i-i collisions, and ζ_3 describes the random processes for i-e collisions with energy exchange. $\mathbf{u}_i$ is the ion mean (fluid) velocity, Z is the average ion charge. All macroscopic values are determined in the "kinetics" cell. The Coulomb logarithms Λ,Λ' for i-i and e-e collisions may be different. The ion heating due to electron-ion collisions is exactly equal to the electron cooling for infinite number of particles. For the finite number of particles the energy is conserved because of ergodicity of such systems. It can be demonstrated analytically.

The leap-frog numerical scheme for non-relativistic plasmas used to solve Eq.(2),(3) is the following ($\tau=t\gamma_{ee}$, $\mathbf{E}=e\mathbf{E}/mc\omega_{pl}$, $\mathbf{H}=e\mathbf{H}/mc\omega_{pl}$, v is in terms of v_{Te})

$$\tilde{\mathbf{v}}^{n+1/2} = \mathbf{v}^{n-1/2} - \Delta t\left(\mathbf{E}(\mathbf{r}^n) + \frac{1}{2}(\tilde{\mathbf{v}}^{n+1/2} + \mathbf{v}^{n-1/2})\mathbf{H}(\mathbf{r}^n)\right),$$

$$\mathbf{r}^{n+1/2} = \mathbf{r}^{n-1/2} - \Delta\tau\tilde{\mathbf{v}}^{n+1/2}$$

$$u^3 = (\tilde{v}^{n+1/2})^3 - 3Z^2\frac{m_e}{M_i}\Delta\tau,$$

$$\tilde{\mathbf{u}} = \mathbf{u} + \sqrt{\frac{Z^2\Delta\tau}{u}}\left(\mathbf{p} - \frac{\mathbf{u}(\mathbf{up})}{u^2}\right), \qquad \mathbf{g} = \tilde{\mathbf{u}} - \mathbf{d},$$

$$\mathbf{w} = \mathbf{g} - \Delta\tau\left(4\frac{\mathbf{g}}{g}G(g) - 4\Phi'(g)\frac{4(\mathbf{qg})}{5}\mathbf{g}\right) \qquad (7d)$$

$$\mathbf{v}^{n+1/2} = \mathbf{w} + \sqrt{\frac{\Delta\tau}{w}}\left[\sqrt{\Phi(w)-G(w)}\left(\mathbf{p} - \frac{\mathbf{w}}{w^2}(\mathbf{w},\mathbf{p})\right) + \sqrt{2G(w)}\frac{\mathbf{w}}{w^2}(\mathbf{w},\mathbf{p})\right]$$

$$+\sqrt{\frac{\Delta\tau}{w}}\left[\sqrt{\Phi(w)-G(w)}\left(\mathbf{s} - \frac{\mathbf{w}}{w^2}(\mathbf{w},\mathbf{s})\right) - \sqrt{2G(w)}\frac{\mathbf{w}}{w^2}(\mathbf{w},\mathbf{s})\right] + \mathbf{d}$$

where **d** is the electron mean velocity in a kinetic cell. **s** and **p** are vectors of normally distributed random numbers, $\langle p\rangle=0, \langle p^2\rangle=0.5$. The scheme for ion collisions is the same.

The explicit scheme (7d) provides the energy, the momentum, and the Maxwellian distribution conservation for the number of particles N>100 per a "kinetics" cell and $\Delta\tau<0.01$. The numerical error arises mainly from the random number computing. To improve (7d) the energy and momentum correction can be applied for every "kinetics" cell. Velocity of the particles in the "kinetics" cell is corrected to conserve energy and momentum before and after the calculation of collisions. The correctness of the procedure is determined by comparing the energy and momentum changes before the correction. With such corrections the energy and the momentum of electrons in kinetic cells are conserved automatically, similar to the BC approximation, the Maxwellian distribution is conserved until N>10, $\tau<1$.

The dimensionless units used even for p-polarized wave have a following form [9-15]: a velocity is in c, an energy is in $m_e c^2$, electromagnetic fields are in $e/(m_e c\omega)$, the time is in ω^{-1},a coordinate is in c/ω. In such units the charge density and current are measured in $(\omega_{pl}/\omega)^2$. Here ω, ω_{pl} are the laser and plasma frequencies

2.2 AVERAGE ION APPROXIMATION. INNER-SHELL X-RAY EMISSION

Even during a short laser pulse there are essential collisional ionization of plasma because of high plasma density [14,15]. For example, by using the Lotz formula for collisional ionization cross- section,

$$\sigma_Z \approx 4 \cdot 10^{-14} \xi \frac{\ln(\varepsilon / I_Z)}{\varepsilon I_Z}, \mathrm{cm}^2, \qquad (8)$$

where I_Z is the ionization energy in eV, ξ is the number of equivalent electrons in an ion shell, ε is the electron energy in eV, and assuming that the plasma density N_0 is equal to 5×10^{22} cm^{-3} and electron energies are about 100 eV, we get the ionization time τ_i been equal to $\tau_i = 5 \times 10^{-2} I_Z$ fs and been much shorter than the pulse duration.

In the PIC simulation any ionization process can be included by allowing the change of superparticle charges. Firstly, we introduce the "kinetics" grid along with the grid for the PIC (see, Fig.1). Many PIC cells (> 20) are enclosed into a "kinetics" cell to provide a good statistics for the electron density, the temperature, and the average ion charge. For an ideal plasma the sense of the "kinetics" cell is obvious. The density and the temperature can be really determined within the length that includes at least some free paths of plasma electrons and much exceeds the length of the PIC cell that approximately equals to the Debye length. The "kinetics" grid simply represents the spatial scale length of macroscopic plasma parameters, as the PIC grid represents that of electro-magnetic field. Any process with typical length that is less than the Debye length or the size of the PIC' cell has to be included in the Langeven equation. If the PIC' cell much exceeds the Debye length, the Langevin equation has to be modified to the LB equation (1) to describe the particle scattering by plasma short wave fields.

The change in the electron charge in every "kinetics" cell is calculated by the standard balance equations in the frame of the average ion approximation,

$$\frac{dQ_{ek}}{dt} = N_Z \left[-Q_{ek}\left(R_Z N_e\right) + \sum_{\varepsilon_l > I_Z} q_l v_l \sigma_Z(v_l) + \frac{\alpha}{\tau(I_{z+1}, E_k)} \right], \qquad (9a)$$

where Q_{ek} is the total electron charge in the kth "kinetics" cell, q_l is the charge of lth electron superparticle, the ionization cross-section σ_Z is used in the form Eq.(8).

$$R_Z = CZ^3 / T_e^{9/2}, \qquad C \approx 6 \cdot 10^{-27} \mathrm{cm}^6 \cdot \mathrm{ev}^{9/2} / \mathrm{s}$$

is the three-body recombination rate. Optical field ionization (OFI) can also be included by introducing the optical field ionization probability, $\tau(I_Z, E_k)$ [36], where E_k is an effective electric field in kth "kinetics" cell. In Eq.(9a) α is a normalization constant. The population of excited states is not included in the present model. The ionization energy I_Z is

continuously changed with average ion charge, Z, and is fitted to be equal to the realistic energy at any integer value of Z. The charge (9a) is determined after every time step and redistributed over all ion and electron superparticles belonged to a "kinetics" cell. The charge of the superparticles is changed by adding

$$\Delta q_{ek} = \Delta Q_{ek} / N_{ke}, \qquad \Delta q_{ik} = -\Delta Q_{ek} / N_{ki}, \qquad (9b)$$

where N_{ke} and N_{ki} are the number of the electron and ion superparticles in the cell. The energy of electrons is decreased as,

$$\Delta\varepsilon_1 = N_0 v_1 \sigma_Z(v_1) I_Z \Delta t.$$

to account for the energy utilized for ionization. The recombination heating of plasma electrons in every "kinetics" cell is included in the following form

$$\Delta\varepsilon_R = N_0 R_Z N_e^2 I_{Z-1} \Delta t.$$

The electron temperature, the density, and the average ion charge in a "kinetics" cell are recalculated after every time step.

Two species of charge are attached for every ion superparticle. The first one, Q_{ik}, is the charge of an ion superparticle which is changed in according to Eq.(9). The second, Q_{ik}^0, is constant which is equivalent to an unit ion charge and is used for calculation of the ion charge to include it in the motion equation (2). The electron density is obtained by weighting the electron superparticle charge density in the "kinetics" cell. The similar procedure with Q_{ik}^0 is used to obtain the ion density. The temperature and the mean velocity of the plasma electrons are determined by simply averaging them using the charge of the superparticle as weight.

To evaluate the inner-shell emission the simplified level population equation in the frame of the average ion model can be used in every "kinetics" cell in the following form

$$\frac{dN_A^{(i)}}{dt} = N_0 \sum_{\varepsilon_1 > I_A} \sigma_Z(v_1) q_1 v_1 / q_0 - (\Gamma_A^{(i)} + A_Z) N_A,$$

where N_A is the density of ith hollow ions, where i=z and z+1, and z is the average ion charge, q_1 is the charge density of a superparticle, q_0 is the normalization constant, Γ_A is the autoionization rate ($\sim 2\times10^{15}$ s^{-1}),

$$A_Z \approx 4.8 \cdot 10^8 Z^4, \ s^{-1}$$

is the radiative decay probability. The inner-shell emission intensity is then computed by the equation,

$$I(\varepsilon_A) = A\varepsilon_A \sum_{k,i} N^{(i)}{}_{Ak} h \exp\left[-\sum_{s<k} \sigma^n_{ph} N_0 h\right], \frac{W}{cm^2},$$

where A, ε_A are the radiative probability and energy for the inner-shell transition, h is the size of the "kinetics" cell, where

$$\sigma^n_{ph} \approx 7.9 \cdot 10^{-18} \frac{n\xi}{Z^2} (I_n / \varepsilon_A)^3$$

is the Kramers cross-section for photoionization with I_n the ionization energy from the n shell. For Li-like ions Γ_A=0, and the appearance only few percents of Li-like ions in the plasma drastically increases its X-ray emission. The emission of He- and H-like ions can not be computed by this way.

2.3 TWO WAVE APPROXIMATION

Since a two dimensional simulation needed to take into account all possible absorption processes of 0.1-10 ps pulse laser along with the X-ray emission of multiply charged ions is still impracticable, we try to simplify calculation by reducing the problem to one dimensional. In order to take into account various absorption mechanisms within 1D calculation, we use a two waves approximation (TWA) following [9,12](see, Fig.2) . In this way we expect to treat correctly the collision absorption, vacuum heating, anomalous skin effect, and the resonance absorption.

According to the TWA there are two plane waves in the plasma. Considering laser propagation in the X-Y plane with x axis normal to the target surface, the first wave is the incoming laser field propagating inward the plasma in X-Y plane at an arbitrary angle θ with y axis. The second wave represents the reflected portion of the laser field propagating outward through a plasma at the angle -θ to its surface. The both waves are coupled by the plasma current. The wavefronts,

$$\varphi_\pm = t \pm \sin\theta x + \cos\theta y = \varphi_\pm(x, \tau = t + \cos\theta y), \qquad (10)$$

of both waves are parallel to the plasma surface. The TWA assumes that there is no distortion of such a wavefront during laser-plasma interaction, no backward scattering, and implicitly uses assumption $\omega T>>1$, where ω is the laser frequency, T is the laser pulse duration. The last assumption is valid even for subpicosecond pulse lasers.

The TWA equations are derived from the two dimensional Maxwellian curl equations written in the following form,

$$\frac{\partial H_Z}{\partial y}=\frac{\partial E_{L,X}}{\partial t}+\left(j_X+\frac{\partial E_{ST,X}}{\partial t}\right),\quad -\frac{\partial H_Z}{\partial x}=\frac{\partial E_{L,Y}}{\partial t}+\left(j_Y+\frac{\partial E_{ST,Y}}{\partial t}\right),$$

$$\frac{\partial E_{L,Y}}{\partial x}-\frac{\partial E_{L,X}}{\partial y}=-\frac{\partial H_Z}{\partial t},\quad \frac{\partial E_{ST,X}}{\partial x}+\frac{\partial E_{ST,Y}}{\partial y}=\rho,\ \frac{\partial j_X}{\partial x}+\frac{\partial j_Y}{\partial y}=-\frac{\partial \rho}{\partial t}, \qquad (11)$$

where L marks a laser field and ST denotes the plasma electrostatic field. In the vacuum the fields are determined by the following equations:
the incoming from right side wave (laser fields),

$$H_Z=H_0\cos(t+\sin\theta x+\cos\theta y+\varphi_0),$$

$$\mathbf{E}=(E_{0x}\mathbf{i}-E_{0y}\mathbf{j})\cos(t+\sin\theta x+\cos\theta y+\varphi_0),$$

$$E_{0x}=H_0\cos\theta, E_{0y}=H_0\sin\theta,$$

the outgoing to the right side (reflected laser fields),

$$H_Z=H_1\cos(t-\sin\theta x+\cos\theta y+\varphi_1),$$

$$\mathbf{E}=(E_{1x}\mathbf{i}+E_{1y}\mathbf{j})\cos(t-\sin\theta x+\cos\theta y+\varphi_1),$$

$$E_{1x}=H_1\cos\theta, E_{1y}=H_1\sin\theta,$$

Here ϕ_0, ϕ_1 are constants.

In the frame of the TWA the following equations are obvious,

$$E_{ST,Y} = 0, \qquad \frac{\partial j_Y}{\partial y} = 0,$$

and the laser field is the function of variables x and τ=t+ycosθ. In terms of the variables τ,x, Eq.(11) can be reduced to the one dimensional form,

$$\cos\theta \frac{\partial H_Z}{\partial \tau} = \frac{\partial E_{L,X}}{\partial \tau} + \left(j_X + \frac{\partial E_{ST,X}}{\partial \tau} \right), \quad -\frac{\partial H_Z}{\partial x} = \frac{\partial E_{L,Y}}{\partial \tau} + j_Y, \tag{12a}$$

$$\frac{\partial E_{L,Y}}{\partial x} - \cos\theta \frac{\partial E_{L,X}}{\partial \tau} = -\frac{\partial H_Z}{\partial \tau}, \quad \frac{\partial E_{ST,X}}{\partial x} = \rho, \frac{\partial j_X}{\partial x} = -\frac{\partial \rho}{\partial \tau}.$$

By excluding $E_{L,X}$ from 1st and 3nd equations of Eqs.(12a) and by introducing H_0=sinθH_Z we get,

$$-\frac{\partial H_0}{\partial x} = \sin\theta \frac{\partial E_{L,Y}}{\partial \tau} + j_Y \sin\theta, \qquad \frac{\partial E_{L,Y}}{\partial x} - \left(j_X + \frac{\partial E_{ST,X}}{\partial \tau} \right) \cos\theta = -\sin\theta \frac{\partial H_0}{\partial \tau},$$

$$E_{L,X} = H_Z \cos\theta + \int_0^\tau d\tau' \left(j_X + \frac{\partial E_{ST,X}}{\partial \tau'} \right), \frac{\partial E_{L,X}}{\partial x} = \frac{\partial H_Z}{\partial x} \cos\theta, \quad \frac{\partial E_{ST,X}}{\partial x} = \rho, \tag{12b}$$

Eq.(10b) can be rewritten in the form of two plane waves,

$$\frac{\partial}{\partial x} A_\pm \pm \sin\theta \frac{\partial}{\partial \tau} A_\pm = -\frac{1}{2} j_Y \sin\theta \mp \frac{1}{2} \cos\theta \left(j_X + \frac{\partial E_{ST,X}}{\partial \tau} \right),$$

$$H_Z = (A_+ + A_-)/\sin\theta, E_{L,Y} = A_+ - A_-,$$

$$E_X = E_{L,X} + E_{ST,X}, \qquad E_{L,X} = (A_+ + A_-)\cos\theta / \sin\theta, \tag{12c}$$

$$\frac{\partial (1+\chi) E_{ST,X}}{dx} = \rho,$$

where A_+ and A_- are the fields of the incoming and outgoing waves moving with velocity of -sinθ and sinθ in the x direction respectively, χ is the implicit susceptibility [36,37]. The absorption efficiency η is determined by the following equation,

$$\eta = 1 - \int dt A_-^2(t,x) / \int dt A_+^2(t,x).$$

The equations (12) exactly correspond to the one dimensional approximation [9] used a relativistic references frame moving with u_y=-cosθ. This can be shown by substituting to the Maxwellian equations in the relativistic reference frame the fields, current components, and the charge density determined in the laboratory reference frame,

$$E_X^{Rl} = (E_X^{Lb} - H_Z^{Lb}\cos\theta)/\sin\theta,\ H_Z^{Rl} = (H_Z^{Lb} - E_X^{Lb}\cos\theta)/\sin\theta,\ E_Y^{Rl} = E_Y^{Lb},$$

$$j_Y^{Rl} = (j_Y^{Lb} + \rho\cos\theta)/\sin\theta,\ j_X^{Rl} = j_X^{Lb}\ \rho^{Rl} = (\rho^{Lb} + j_Y^{Lb}\cos\theta)/\sin\theta,$$

where the Lb marks the values in the laboratory frame and the Rl in the relativistic frame. However the laboratory reference frame is much preferable for non-relativistic plasmas letting us avoid a noise due to appearance of the plasma charge density in the Maxwellian curl equations. Equations (12c) are the well known s-wave equations [36] at $\theta=\pi/2$.

The boundary conditions for Eq.(11) are trivial. The incoming field is equal to laser' at the right side, and outgoing field is zero at the left side. The plasma electric field outside the simulation box is zero.

2.4 PARTICLE-IN-CELL PORTION

To solve Eqs. (2), (7), and Eq. (12) the 1D3V relativistic electromagnetic code [17] with the square weighting for the current and charge is used. Both the direct-implicit (C1) scheme [37] and the leap-frog scheme [36] are employed. We could not use completely the advantage of the direct-implicit scheme because of a high laser frequency. Collisions are computed as an effective force after calculation of the velocity and the position of particles. The kinetic parameters such as the temperature and the densities are determined on the "kinetics" grid for every calculation step.

2.5 BOUNDARY CONDITIONS

The boundary conditions for superparticles in the system under consideration are not trivial. In the present calculation a superparticle accelerated over the system boundary in the laser side is kept at zero x-component velocity all the rest time. The charge of such a

superparticle is involved in the electrostatic field calculation. The velocity of a superparticle accelerated over the system boundary in the plasma side is redistributed within the Maxwellian velocity distribution with the initial plasma temperature.

3. RESULTS OF SIMULATION

To demonstrate the ability of the method presented here first of all the heat flow in a uniform plasma initially with a steep temperature gradient is considered.

3.1 A STEEP TEMPERATURE GRADIENT DECAY

Firstly we have conducted the simulation of a steep temperature gradient decay following [16,17] (see also [38]). Both electron-electron and electron-ion Coulomb collisions are included in the simulation.

Three numerical schemes have been employed. The leap-frog scheme, and the direct implicit schemes C1,D1 [37]. To demonstrate the accuracy, temporal evolution of the total energy calculated using two direct implicit schemes are presented in Fig.3. As possible to see, even at low energy the accuracy within 10% is kept during t= $2000/\omega_{pl}$. Such accuracy is enough for the simulation of short pulse laser -plasma interaction.

We have calculated temporal evolution of the temperature distribution, and plotted the heat flux as a function of the local temperature gradient, as shown in Fig.4-6. Calculations are carried out by setting initial condition as the temperature at the left boundary is 4 times higher than that at the right boundary. The size of the system is approximately 100 free electron paths, and the number of electrons in the Debye sphere is set to 10. The average plasma charge is constant and set to be equal to 4. Two different boundary conditions are considered. In the first calculation, the heat flux across the boundary is set to zero so that total energy in the system is conserved. The instantaneous distribution of the plasma temperature and the heat flow after certain time are shown in Fig.4 a,b and Fig.5 a,b.

Obviously the temperature which initially has a steep gradient relaxes to smooth spatial profile. In the next calculation, the temperature at the boundaries are kept fixed. The velocity of the electrons which approach the boundary is redistributed according to Maxwellian distribution. The results of the simulation with and without electron- electron collisions are presented in the rest of Fig.4,5. The temperature distribution, initially steep, in that case almost approach to the steady-state distribution after 400 plasma periods that approximately correspond to 80 electron-ion collisions. For ion charge Z=4 the electron-electron collisions do not change the temperature evolution and the heat flow

because no atomic process is included. The heat flow distribution itself is numerically and qualitatively similar to one in [16]. The plot of the local heat flow versus inverse local temperature gradient is presented in Fig.6a. The ratio of the local heat flow, which is averaged over time of few collisions, to the Spitzer-Harm heat flow determined by a local temperature gradient is quantitatively correspond to results [16], [17]. In the case of the steep temperature gradient, the heat flux shows strong inhibition corresponds to that shown by previous Fokker-Planck simulations. However, due to difficulty of determination of the temperature gradient (numerically incorrect problem for any PIC simulation), the heat flux doesn't show clear correspondence with classical values for longer temperature gradient. The Fig.6b shows the temperature distribution after long time when the profile gets to a steady-state. The distribution is very close to the steady-state distribution which is determined by the Spitzer-Harm heat conductivity

$$\frac{T_e(x)}{T_0}=\left[\frac{x}{L}+\left(\frac{T_1}{T_0}\right)^{\frac{7}{2}}\left(1-\frac{x}{L}\right)\right]^{2/7},$$

where L is the plasma length, $T_1>T_0$ are the temperature of the plasma at its edges.

3.2 HEAT FLOW AND IONIZATION DYNAMICS IN PLASMAS IRRADIATED BY LASER PULSE

The present calculations of subpicosecond pulse laser-plasma interaction are carried out for silicon and carbon plasmas of solid-density $N_{solid}=5\times10^{22}$ cm^{-3}. The plasma size is varied from 0.25 μm to 1 μm depending on the laser intensity and its polarization. The two plasma density profiles on the target surface, at the right (laser) side of plasma are chosen for the simulation. The first is a linear profile,

$$N(x)=N_1\left(1-\frac{N_{cr}}{N_1}\frac{x}{L}\right),\ N_{cr}<N_1<N_{solid}. \qquad (13a),$$

and the second is an exponential profile,

$$N(x)=N_1e^{-\frac{x}{L}},\ N_1\approx N_{solid}, \qquad (13b),$$

where L is the density gradient in the vicinity of the critical density N_{cr}. $N(x<0)=N_1$. The presentations (13) for the plasma density are good approximations for density profile formed after plasma expansion due to laser prepulse (see, Fig.7). The value of L determined

by the prepulse delay is varied from 0.0 μm to 0.6 μm. The initial electron temperature is chosen equal to 10 eV and to 20 eV for silicon and carbon plasmas respectively. The initial velocity distribution of plasma electrons is the Maxwellian. The fluid velocity linearly increasing toward the plasma surface is suggested. Initially the ion charge is uniform over all plasma, and the ion and electron densities are equal. The laser wave length, the duration, the intensity, and also L are the parameters.

To provide stability the number of superparticles used is around 70,000 per 1 μm of a plasma. The number of the PIC cells is varied from 8000 to 16000, the number of the "kinetics" cells is varied from 200 to 600. The time step is varied from the initial value of 0.1 to 0.36 of the plasma oscillation period due to the ionization. The plasma bulk in the simulations is divided into two parts, in accordance with Eq.(13), and two different species of superparticles are used for the simulation. The charges of the superparticles which represent electrons and ions for each kinetics cell are changed following the rule described in the previous section. The intensity of the laser pulse is constant.

3.2.1 HEAT FLOW AND IONIZATION DYNAMICS IN PLASMAS IRRADIATED BY S-POLARIZED PULSE

Calculations of the heat flow and the ionization dynamics in a plasma irradiated by s-polarized subpicosecond laser pulse using PIC&Langevin simulation provides a good check of the method by comparing the results with those obtained from direct solution of the FPL equation.

Following [15] we consider a solid density carbon plasma irradiated by the s-polarized pulse of KrF laser (λ=248 nm). The initial temperature of the plasma is chosen to be 20 eV and initial ion average charge is set to Z=1.3. In contrast to Town and Bell' simulation, instead of assuming the amount of energy deposited in the plasma surface, the laser intensity is chosen for the deposited energy to be equal that used in [15] (750 TW/cm^2 x 300 fs). We have chosen I=10^{16} W/cm^2. The very steep density gradient at the plasma surface, L=0, is considered. Both electron-electron and electron-ion collisions are involved in the simulation in the frame of the Langevin equation (2),(3) because the collisional absorption in this case is the dominant.

The results of the simulation are presented in Fig.8,9. The temporal evolution of the absorption coefficient and the portion of absorbed energy spent for plasma electron heating including the energy of electrostatic field is shown in Fig.8. The absorption coefficient is very close to that used in [15], 7.8%. At the beginning of the heating process the ionization takes a large portion of the absorbed laser energy. After the average ion charge exceeds 4

(Li-like carbon) the energy of plasma electron is not enough for efficient ionization of He- and H-like ions. Then the deposited laser energy is mainly utilized by plasma electrons through the heat transfer.

Spatial and temporal evolution of the plasma temperature and the electron density inside plasma is shown in Fig.9. Initially the heating occurs only in the skin layer determined by electron-ion collision. The energy of the quiver in this case is not high, approximately 50 eV, and a certain time is need for plasma heating. As the average ion charge in the skin layer is increased due to the electron collisional ionization, the heating in the skin layer increases too so the collisional time is almost fixed. Ionization decreases the skin layer length because of continuously increasing of the plasma frequency in the skin layer. As a results of ionization the reflectivity increases. It means that ionization dynamics not only affects on the heat flow but also on the plasma reflectivity.

In Fig. 9 c,d electron temperature and density inside the plasma calculated by present simulation are compared with the results of previous FP calculation [15] to show brilliant agreement.

We should point out that electron-electron collisions do not notably affect on the absorption efficiency and the ionization balance because of the high average ion charge ($Z>4$) in the heated skin layer, but we have to maintain such collisions in the model to properly include ionization and recombination processes in the low temperature plasma background. At higher intensity, generation of fast electrons and successive modification of density gradient may have significant effect on laser-plasma interaction, so that self-consistent calculation of the laser absorption and the heat flow will become more important.

3.2.2 ABSORPTION OF A P-POLARIZED PULSE LASER

The self-consistent simulation of the absorption of a p-polarized pulse laser by solid density plasmas along with ionization dynamics has not been carried out, although it is obvious that the ionization process may affect not only on the heat flow but also on the plasma reflectivity. In the present work the hybrid particle-in-cell method is applied to model the absorption of p-polarized pulse laser for the parameters of the experiment [30], λ=800 nm and the intensity $I=4\times10^{16}$ W/cm^2 for silicon plasma. The calculations are carried out for various density gradients and incident angles.

The one dimensional calculation of the laser field in the case of its p- polarization is not trivial (see, for example, [9], [12]). The typical results of the calculation by the TWA, when the resonance absorption occurs, are presented in Fig.10. The averaged distributions

of the fields are similar to that obtained by P.Gibbon [12]. Due to the resonance absorption, the x-component of the electric field is compressed in the vicinity of the critical density and accelerates a part of the plasma electrons outward plasma. The electrostatic field directed outward the plasma grows then, and low energy electrons can not leave plasma. As the ion charge Z increases the return current decreases as 1/Z due to the increase of electron-ion collision rate. Therefore, the electrostatic field in the plasma increases resulting in the higher energy of fast electrons.

The result of the anomalous skin effect, vacuum heating, and collisions in the absorption efficiency can be estimated for the steep density gradient plasma (see, [6] and references there). So, the efficiency due to the anomalous skin effect is

$$\eta \approx \left(\frac{v_{T_e} \omega^2}{c \omega_{pl}^2} \right)^{1/3},$$

and, for the parameters of [30], is about 10%. The efficiency of the vacuum heating [7],

$$\eta \approx 3 \frac{\cos^3 \theta}{\sin \theta} \frac{v_{os}}{c},$$

where v_{os} is the quiver velocity, is small, around few percents. The efficiency of the collisional absorption,

$$\eta \approx \frac{2\omega}{\omega_{pl}} \left(\frac{\gamma_{ei}}{\omega_{pl}} \right)^{1/2}, \gamma_{ei} > \omega,$$

(γ_{ei} is the collision frequency) is also similar to that of the anomalous skin effect, 10%. Consequently, the total efficiency owned to these processes is hardly higher than 20%. The results of the simulation of the s- and p- polarized pulse absorption by a plasma with very steep density gradient without ion motion is in good agreement with the estimations

Fig.11 illustrates the evolution of the absorption efficiency for the plasma with different density gradient in the vicinity of the critical density. The linear density profile is determined by Eq.(13a). Such a distribution is close to that obtained by a solution of the hydrodynamic equation for an initially steep distribution of the electron temperature (Fig.7). We obtained the maximum absorption efficiency (η=67%) at N_1= 1.2×10^{22} cm^{-3}, L=0.22 μm, and the incident angle at 45^o. If initially plasma boundary were heated by a laser prepulse to have

an expansion velocity of $(1\text{-}2)\times10^7$ cm/s it would pass through the distance $S= N_1L/N_{cr}$ within τ=4-8 ps. Any change in the angle, density, or the length L leads to decreased absorption efficiency that justifies the resonance character of the absorption. Fig.12 illustrates the evolution of the absorption efficiency at different incident angles. The absorption efficiency decreases with incident angle to a limiting value which is determined by the collisonal absorption, anomalous skin effect, and the vacuum heating. The simulation has reproduced the results [9] in the absent of collisions and ion motion.

The results of the calculation of the absorption efficiency for exponential density profile, Eq.(13b), are plotted in Fig.13. As in the case of the linear density profile the absorption has the resonance character. The maximum of the absorption is obtained at the density gradient L=0.17 μm that coincides with the result obtained for the linear density distribution. That parameters correspond to prepulse duration of 4-8 ps. The results also show that in the case of exponential profile the plasma can loss the resonance condition during the laser pulse. Then absorption efficiency decreases. The difference in the absorption efficiency for s- and p- polarized pulses for the plasma with very steep density gradient (see, Fig.13) is due to Brunel's vacuum heating [7]. This process also is responsible for fast electron generation in very steep density, collisionless plasmas (see, 3.2.3).

To verify the effect of ion motion on the plasma reflectivity the plasma ion are allowed to move in the self-consistent field. The ionization process must lead to considerable acceleration of heavy plasma ions by the compressed electric field, because of high ratio of $Z/M_i<1/3m_H$ (m_H is the hydrogen atom mass) , that results in the resonance absorption process [12]. The typical evolution of the ion density during laser-plasma interaction (within 120 fs) is shown in Fig.14a,b. Ion-ion collision is not included in this calculation. As possible to see there is no notable ion motion in the vicinity of the critical density during laser-plasma interaction t<120 fs. It means that the effect of ion acceleration by the electrostatic field is hardly responsible for the absorption increasing with the laser prepulse. Only in the case of the very steep density gradient, the absorption efficiency is changed a little due to the ion motion. In this case, the electrons ionize the plasma up to Z=10 to cause higher electric field and faster ion motion. Nevertheless, the density gradient in the vicinity of the critical density is still far from the optimal to increase the absorption. The effect of ion motion increases with laser intensity (see Fig.13). But even for intensity $I=4\times10^{17}$ W/cm^2 the absorption efficiency is as twice as less the maximal. Initial fluid velocity of the plasma is also varied from 0 up to 2×10^7 cm/s in the calculations to show no effect on the absorption efficiency.

The effect of variable ionization is illustrated by Fig.15. Both in the case of the linear and exponential density gradient the calculation with fixed ion charge results with a lower

absorption efficiency. The gradual decrease of the absorption in the case of the exponential density distribution with fixed ion charge, Z=1, demonstrates disability of the ion motion to maintain the resonance absorption conditions for such a short pulse laser.

Fig.16 represents the dependence of the measured [30] and computed reflectivity of a silicon plasma for the different density gradient in the vicinity of the critical density (a) and the prepulse delay (b). The latter was plotted using the measured dependence of the density gradient on the prepulse delay [30]. The numerical results are in a good agreement with the experimental ones when the resonance absorption occurs. For the very steep density gradient the numerical absorption efficiency (28%) is less then the measured (35%) in Ref.[30]. But for shorter prepulse delay the result of the simulation is very sensitive to variation of the density gradient. With prepulse delay τ=1.5 ps or L/λ=0.1 the numerical efficiency increases up to 50% for the exponential density distribution. Thus any heating of the very steep density plasma before the laser pulse can change the absorption efficiency.

3.2.3 HEAT FLOW IN PLASMAS IRRADIATED BY P-POLARIZED PULSE

Calculation of the heat flow in the case of irradiation by an intense, p-polarized pulse laser is carried inward plasma by fast electrons produced by collisionless absorption processes. Firstly, we estimate the penetration depth assuming that all of whole deposited power, W, is taken off by fast electrons with energy $<\varepsilon>$,

$$W = \eta I = < \varepsilon > j_{fast} / e, \tag{14a}$$

where η is the efficiency, I is the laser pulse intensity, j_{fast} is the density of the fast electron current. To provide the plasma neutrality the fast electron current must be compensated by the plasma current, j_{pl},

$$j_{fast} = j_{pl} = \frac{e^2 E N_e^{solid}}{m_e \gamma_{ei}}, \tag{14b}$$

where E is the electric field in the plasma, γ_{ei} is the electron-ion collision frequency. According to Eq.(14b) the density of the deposition energy can be found by following equation

$$\frac{dW}{dx} = -j_{pl} E = -W^2 \frac{m_e \gamma_{ei}}{N_e^{solid} < \varepsilon >^2}, W(0) = \eta I. \tag{15}$$

The deposition depth can be easily estimated by solving Eq.(15)

$$l_D = \frac{N_e^{solid} < \varepsilon >^2}{\eta I (m_e \gamma_{ei})} = \frac{m_e v_{T_e}^3 < \varepsilon >^2}{4\pi \Lambda \eta I e^4 < Z >}$$

For T_e=100 eV, <Z>=1, <ε>=3 keV, I=4x10^{16} W/cm^2, and η=0.3 the depth is 0.1 μm. Since the ratio $<\varepsilon>^2$/I weakly depends on the intensity, the value of the depth is mainly determined by the temperature of a solid density plasma. An increasing in the average ion charge leads to a decreasing of the deposition depth.

The plasma temperature and the electron density distributions in the plasma after laser pulse are presented in Fig.17-20. Fig.17 represents the results of the electron temperature and the density calculation in the collisionless plasma (Fig.17 a,c) and in the plasma with elastic electron-ion and electron-electron collisions (Fig.17 b,d) without ion motion. The efficiency of the absorption due to collisionless processes such as the anomalous skin effect and the vacuum heating is not small (see, 3.2.2) , about 10%, and is almost equal to the efficiency of the collisional absorption. Absence of elastic collisions decreases the absorption efficiency approximately by 2 times. Distributions of the electron temperature and density inside the collisionless plasma are totally different from those inside a plasma with elastic collisions. This is a result of the very small resistivity of a collisionless plasma. The fast electrons produced by the vacuum heating [7] can easily penetrate into the plasma bulk. In contrast, the fast electrons in the collisional plasma, been decelerated by the internal electrostatic field which arises because of the plasma resistivity, deposit their energy near the plasma surface. The fast electrons produce the return current to hold the plasma neutrality. The energy of electrons in the return current is much less than that of the fast electrons, but higher than the ionization energy. As a results the ionization by the return current electrons is much more efficient. This means even if the absorption due to the vacuum heating or due to the resonance absorption is dominant the ionization balance and the heat transfer into an overdense plasma, and, as a result, its X-ray emission, can be determined by elastic collisions.

The electron temperature (a) and density (b) distributions obtained without electron-electron collisions are presented in Fig.18 for the parameters near the optimal absorption. The dominant portion of the absorbed laser energy is deposited in the low density plasma. The fast ionization in the solid density plasma leads to the increased electron-ion collision frequency because of high ion charge and relatively low electron temperature. As a result,

the penetration depth does not increase during laser pulse. Fig.19,20 illustrate the effect of the electron-electron collision on the temperature and electron distributions in the solid density plasma. The abundance of the fast electrons in the vicinity of low temperature, high density plasma due to electron-electron collisions increases the plasma conductivity and , as a result, increase the penetration depth of fast electrons produced by the resonance absorption.

The temporal evolution of the electron temperature and density for higher laser intensities are presented in Fig.21. During initial 150 fs (t=300) of the laser pulse the temperature and density evolution is determined by the anomalous skin effect. The plasma electrons are heated up very quickly to 1 keV at the solid surface, and the ions are stripped to N-like and B-like states. Then ionization runs slowly because the number of electrons which are able to ionize ($\varepsilon > I_Z$) decreases and because the ionization time $\tau \sim I_Z^{3/2}$ increases. The heat transfer is determined by fast electrons accelerated by the vacuum heating and $\mathbf{E} \times \mathbf{H}$ force. Due to the high plasma resistivity the penetration depth is small, around 0.5 μm. When the resonance absorption rises because of ion motion (see Fig.13) the heat transfer is increased. The high energy electron ($\varepsilon > 10$ keV) appear in the vicinity of the critical density and penetrate into the plasma flattening the temperature distribution near the surface. Although the absorbed energy is high enough to fully ionize plasma ions, only Li-like ions exist because the time of 200 fs is not enough for further ionization.

4. SUMMARY

The three approaches are suggested to simulate the heat transfer and ionization dynamics for solid-density plasma irradiated by a subpicosecond laser pulse of arbitrary polarization:

-the 1D particle-in-cell method in conjunction with the use of the Langevin equation for electron elastic collisions that conforms to a direct solution of the Fokker-Plank-Landau equation;

-the two wave approximation allows the p-polarized laser-plasma interaction simulation in the laboratory reference frame;

-the method of redistribution of variable superparticle charges into the "kinetics" grid cells to include the atomic physics processes in the PIC simulation.

The method has been applied to simulate the relaxation of the steep temperature gradient , where the heat conduction becomes non-local. It is found that the heat flux approaches to ~0.1 of the free streaming flux in the limit of very steep temperature gradient, and to the Spitzer-Harm in the limit of a steady state. The results of calculation is close to that from FPL simulation [16,17].

The method has been used also for simulation of the heat transfer in a carbon plasma, with elastic collisions and variable ionization, irradiated by s-polarized pulse of KrF laser. The laser absorption was computed self-consistently. The spatial distribution of the electron density and temperature after t=0.3 ps of laser irradiation is in an excellent agreement with those obtained by the direct FPL simulation [15].

The effect of elastic collisions and the variable ionization on the absorption efficiency for Si solid density plasmas have been explored. The results of the present simulation showed a good agreement with the results of the previous simulations of the absorption efficiency of collisionless plasmas by the PIC [9,12]. The calculation of the absorption efficiency of the p-polarized laser showed that the absorption is mainly determined by the vacuum heating and anomalous skin effect with a steep density gradient and later it is dominated by the resonance absorption as the density scale length near the critical surface increases. The absorption efficiency of an s-polarized pulse is almost half the absorption of a p-polarized pulse. The inclusion of elastic collisions increases the absorption efficiency about two times due to the collisional absorption. If the density gradient in the vicinity of the critical density $L/\lambda>0.1$, the resonance absorption becomes dominant, increasing the absorption efficiency up to 65%. The ionization of the plasma has effects on the absorption efficiency both via the ion acceleration and via the collisional absorption. Because of large charge of ions their acceleration is efficient, and a lower density plasma is created. However, for considered short pulse the gradient scale length of the plasma near critical surface does not become long enough ($L/\lambda>0.1$), within the pulse duration of the laser, for efficient resonance absorption. The absorption efficiency of a p-polarized pulse with intensity $I=4\times10^{16}$-4×10^{17} W/cm^2 for Si plasmas with a steep density gradient only increased up to 30% due to ion motion.

The effect of variable ionization and elastic collisions is found to change the heat transfer process by fast electrons into the overdense plasma by changing the plasma conductivity. Due to collisions, the penetration depth of fast electrons is much smaller than that of collisionless plasmas. The electron-electron collisions lead to efficient ionization by electrons in the return current.

ACKNOWLEDGMENTS

The authors would like to thank Professor T.Tajima, whose comments led this work,
Dr. Y. Kishimoto for fruitfull discussions and comments for the PIC simulation,
and Dr. H. Ihara, Dr. Y. Ueshima, and Dr. K. Moribayashi for useful discussion,
and Dr. T. Arisawa for encouraging this research.

REFERENCES

1. Cobble J.A., Schappert G.T., Jones L.A., Taylor A.J., Kyrala G.A., and Fulton R.D.: J. Appl. Phys. 69, 3369 (1991).
2. Rouse A.,Audebert P.,Geindre J.P.,Fallies F.,GauthierJ.C., Mysyrowicz A., Grillon G., Antonetti A.: Phys. Rev. E50, 2200 (1994).
3. Feurer T.,Theobald W.,Sauerbrey R.,Uschmann I.,Altenbernd D., Teubner U., Gibbon P., Forster E., Malka G., Miquel J.L.: Phys. Rev. E 56 4608 (1997).
4. Harris S.E., Kmetec J.D.: Phys. Rev. Lett. 61, p.62 (1988).
5. Kauffman R.: "X-ray radiation from laser plasma", Handbook of Plasma physics, Eds. M.N.Rosenblut and R.Z.Sagdeev, Vol.3: Physics of Laser Plasma, ed. A.M.Rubenchik and S.Witkovski, North-Holland, 111 (1991).
6. Gibbon P., Forster E.: Plasma Phys. Contr. Fusion 38, 769 (1996).
7. Brunel F.: Phys. Rev. Lett. 59, 52 (1987).
8. Rozmus W., Tihkonchuk V.T.: Phys.Rev. A42, 7401 (1990).
9. Gibbon P., Bell A.R.: Phys. Rev. Lett. 68, 1535 (1992).
10. Wilks S.C., Kruer W.L., Tabak M., Langdon A.B.: Phys.Rev.Lett. 69,1383 (1992).
11. Denavit J.: Phys.Rev.Lett. 69, 3052 (1992).
12. Gibbon P.: Phys. Rev. Lett. 73, 664 (1994).
13. T.-Y.Brian Yang,Kruer W.L.,More R.M.,Langdon A.B.:Phys.Plasmas 2, 3145 (1995).
14.Matte J.P.,Keiffer J.C.,Ethier S.,Chaker M.,Peyrusse O.:Phys.Rev.Lett. 72,1208 (1994).
15. Town R.P., Bell A.R., Rose S.J.: Phys. Rev. Lett. 74, 924 (1995).
16. Bell A.R., Evans R.G., Nicholas D.J.: Phys. Rev. Lett. 46, 243 (1981).
17. Matte J.P.,Virmont J.: Phys.Rev.Lett. 49, 1936 (1982).
18. Ivanov M.F., Svets V.F.: Sov.Phys. Dokl., 23, 130 (1978)
19. Zhidkov A.G., e.a.: Laser Physics 4, 1131 (1994)
20. Zhidkov A.G.: Phys. Plasmas 5, 385 (1998).
21. Cadjan M.G., Ivanov M.F.: Phys. Lett.A 236, 227 (1997)
22. Jones M.E., Lemons D.S., Mason R.J., Tomas V.A., Winske D.: J.Comput.Phys.123, 169 (1996)
23. Manheimer W.M., Lampe M., Joyce G.: J.Comput. Phys.,138, 520 (1997)
24. Lampe M., e.a.: Langevin/Monte Carlo treatment of Coulomb collisions in PIC simulation, Proceedings of 16th Int. Conf. on the Numerical Plasma Simulation, US (1998)
25. Jones M.E., Lemons D.S., Winske D.: Improved Intra-Species Collision Models for PIC Simulation, Proceedings of 16th Int. Conf. on the Numerical Plasma Simulation, US (1998)

26. Cadjan M.G., Ivanov M.F.: Stochastic method for the simulation of plasma kinetic with Coulomb collisions, Proceedings of 16th Int. Conf. on the Numerical Plasma Simulation, US (1998)

27. Birdsall C.K.: IEEE Trans. Plasma Sci. 19, 65 (1991)

28. Nanbu K.: Phys. Rev. E 55, 4642 (1997)

29. Sentoku Y.,Mima K., Kishimoto Y.,Honda M., (to be published)

30. Bastiani S., Rousse A., Geindre J.P., Audebert P., Quoix C., Hamoniaux G., Antonetti A., Gauthier J.C.: Phys. Rev. E 56, 7179 (1997).

31. More R.M.: "Atomic physics of laser-produced plasmas", Handbook of Plasma Physics, Eds. M.N.Rothenbluth and R.Z. Sagdeev, 3, Physics of laser plasma, A.M.Rubenchik and S.Witkovsky, North-Holland, 63 (1991).

32. Balescu R.: Phys. Fluids 3, 52 (1960).

33. Lenard A.: Ann. Phys. 3, 90 (1960).

34. Trubnikov B.A.: "Collision of particles in fully ionized plasma", Reviews in Plasma Physics, ed. by M.A. Leontovich, Consultant Bureau, NY, 1, 95 (1965).

35. Amosov M.V.,Delone N.B. ,Krainov V.P.: Sov.Phys.JETP, 64, 1191 (1986)

36. Birdsall C.K., Langdon A.B.: "Plasma Physics, via Computer Simulation",McGraw-Hill, NY, (1985).

37. Cohen B.I.,Langdon A.B., Hewett D.W.: J. Comput. Phys. 81, 151 (1989).

38. Kishimoto Y., Mima K., Haines M.G.: J. Phys. Soc. Jpn. 57, 1972 (1988)

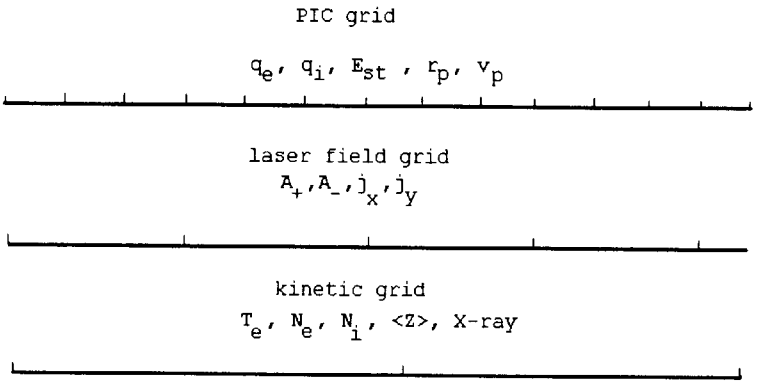

Fig.1 The scheme of different grids that are used for the simulation of subpicosecond pulse laser and solid density plasma interaction. The upper grid is the common used grid for PIC with cell size is around Debye radius. The second grid is for the laser field calculation. The cell size of such a grid is larger than PIC's to avoid the instability produced by high ratio of $\Delta t/\Delta x_{PIC} >> 1$ in calculations. The last grid is the "kinetics" grid for calculation of microscopic parameters of the plasma.

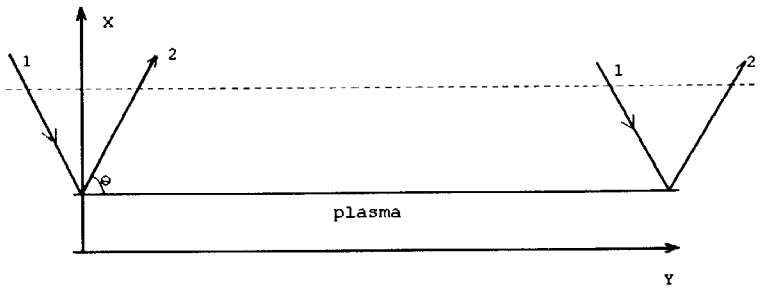

Fig.2 The scheme of the two wave approximation.

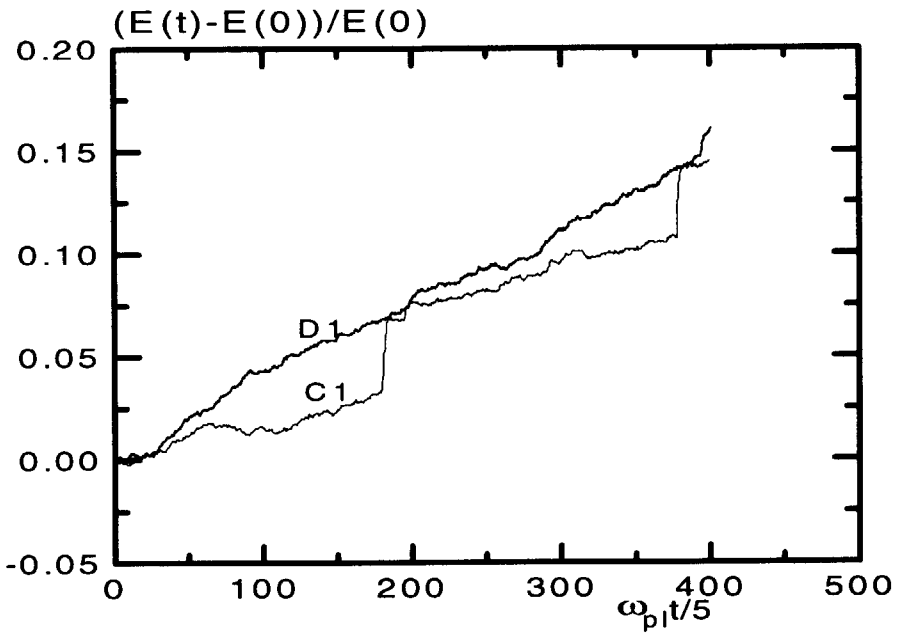

Fig.3 The temporal evolution of the full energy of a plasma due the to numerical heating for D1 and C1 direct implicit schemes [24]. Two open boundary plasma with $T_e(0)$=10 eV, $T_i(0)$=5 eV, N_0=5x10^{22} cm^{-3}, steep density gradients. No laser pulse, electron-electron, electron-ion, ion-ion collisions, no inelastic collisions included.

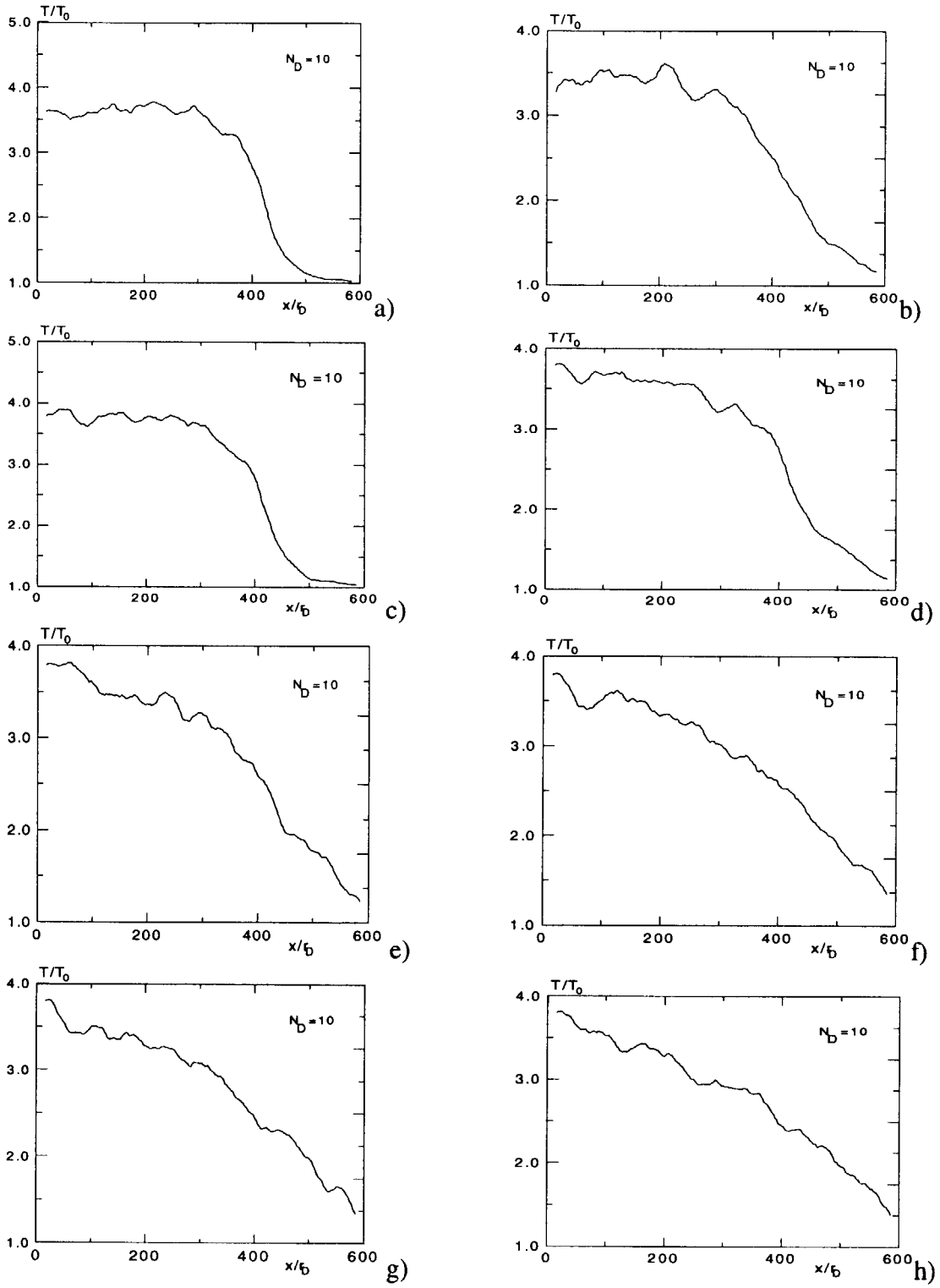

Fig.4 a-h

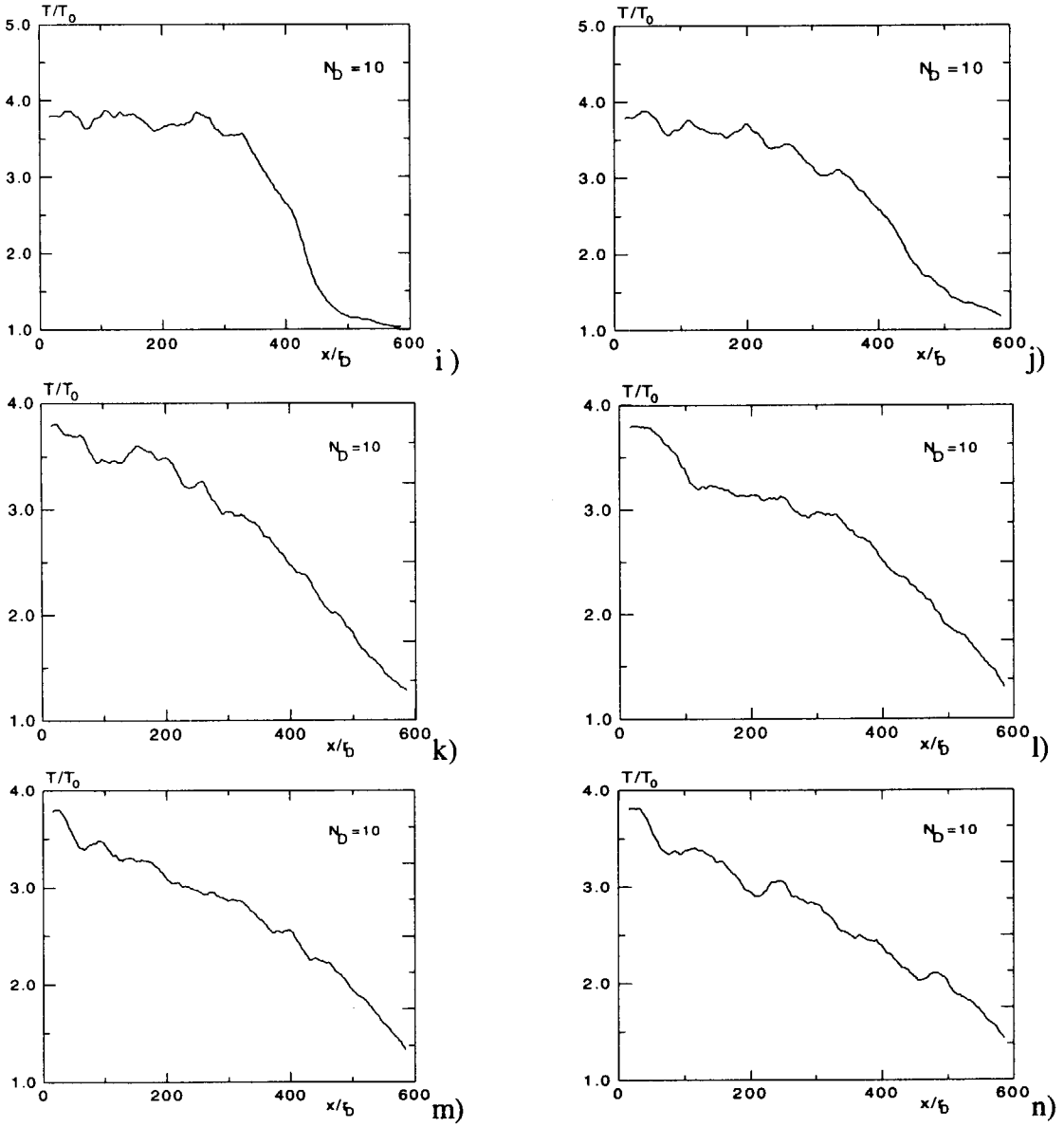

Fig.4 The evolution of the initially steep temperature distribution in a plasma with the number of electrons in the Debye sphere equals 10 and the average charge <Z> equals 4. a) $\tau=t\omega_{pl}=100$, b) $\tau=200$; the temperature at the edge is not fixed, and c,i) $\tau=100$, d,j)$\tau=200$, e,k)$\tau=300$, f,l)$\tau=400$, g,m) $\tau=500$, h,n) $\tau=600$ for the fixed temperature. a),b), c),d),e),f),g) with electron-electron collisions, i),j),k),l),m) without electron-electron collisions.

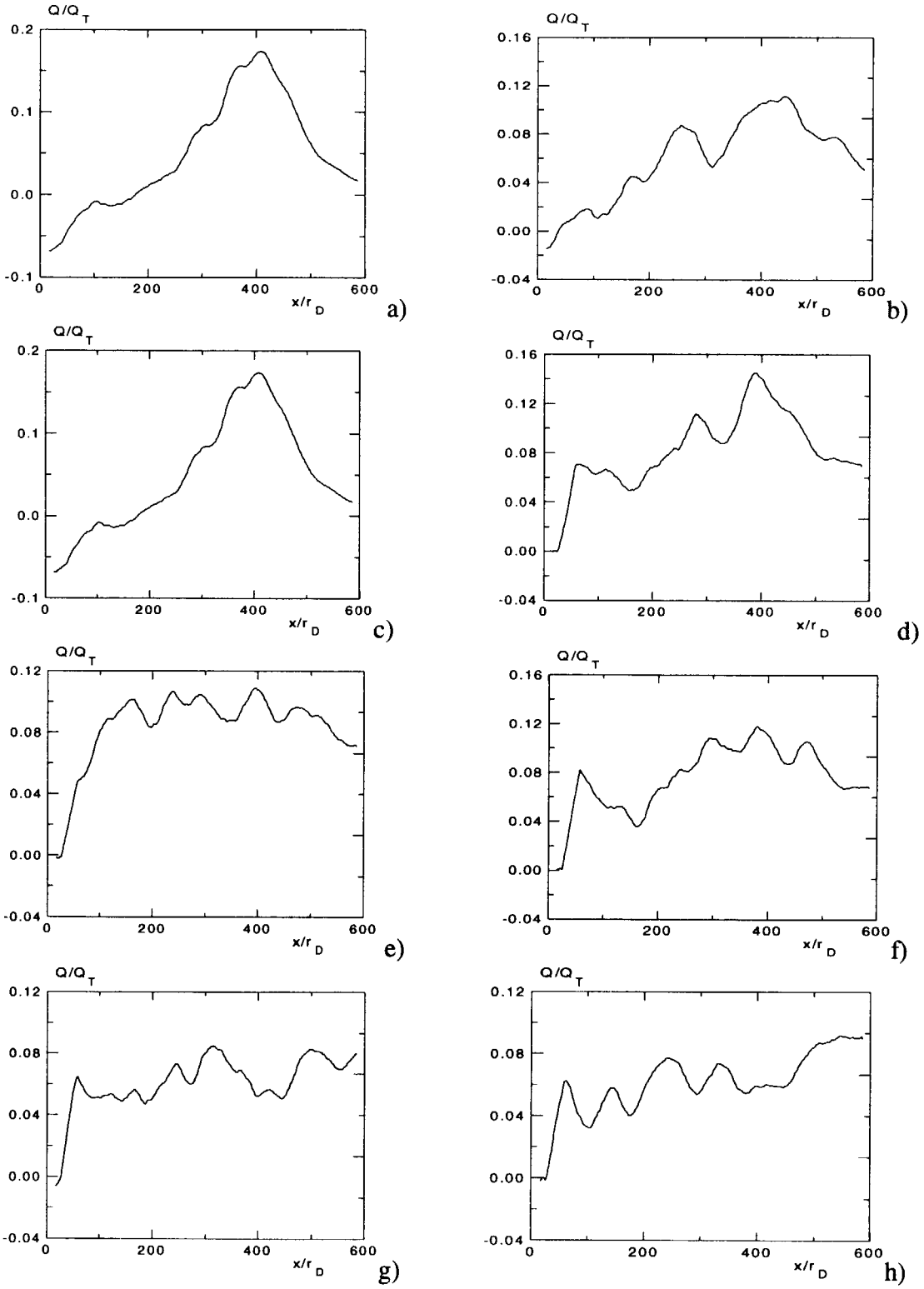

Fig.5 a-h

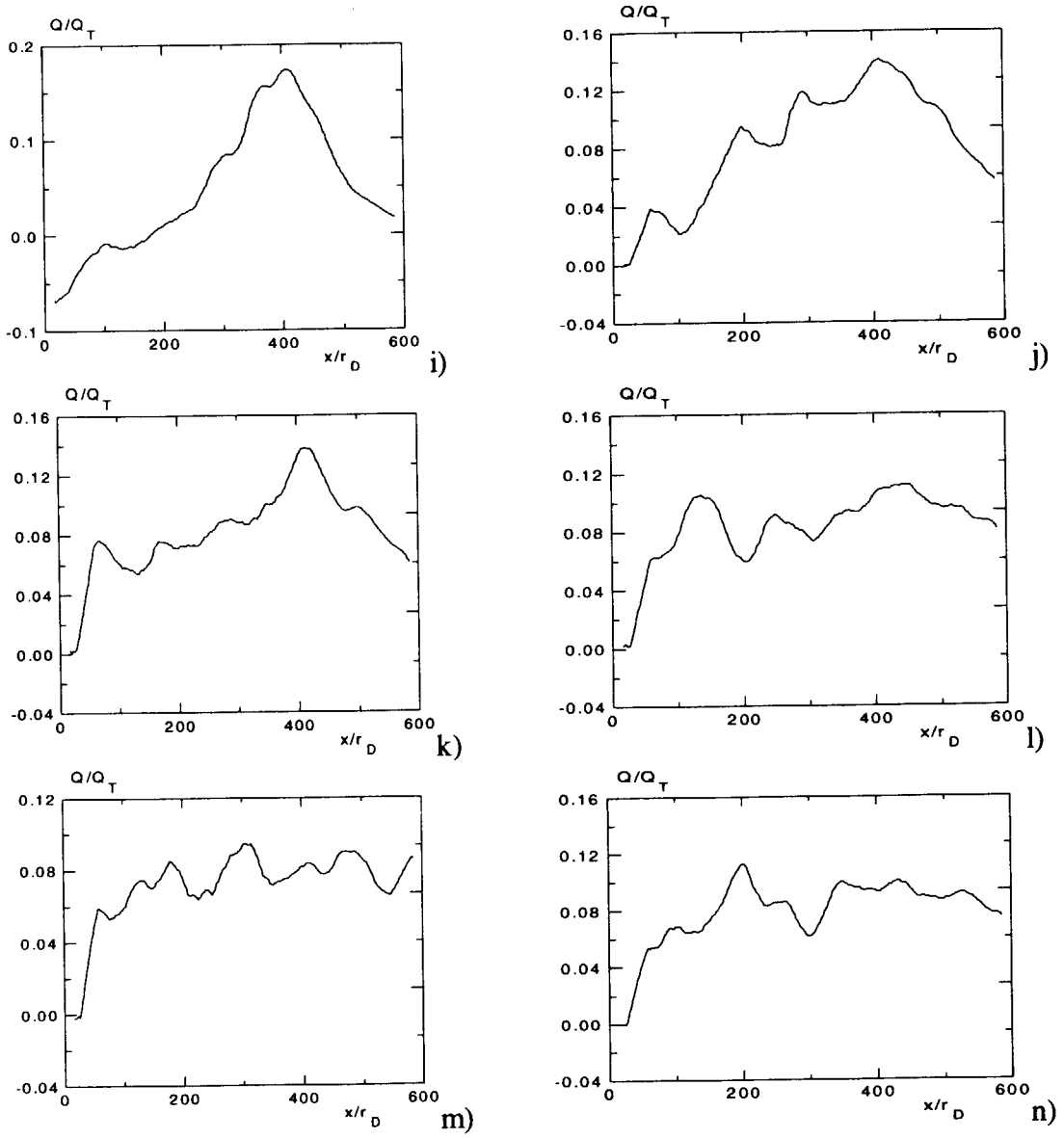

Fig.5 The evolution of the heat flow in the Plasma with parameters given in Fig.3. a) $\tau=t\omega_{pl}=100$, b) $\tau=200$; the temperature at the edge is not fixed, and c,i) $\tau=100$, d,j)$\tau=200$, e,k)$\tau=300$, f,l)$\tau=400$, g,m) $\tau=500$, h,n) $\tau=600$ for the fixed temperature. $Q_T=NT_e(T_e/m_e)^{1/2}$

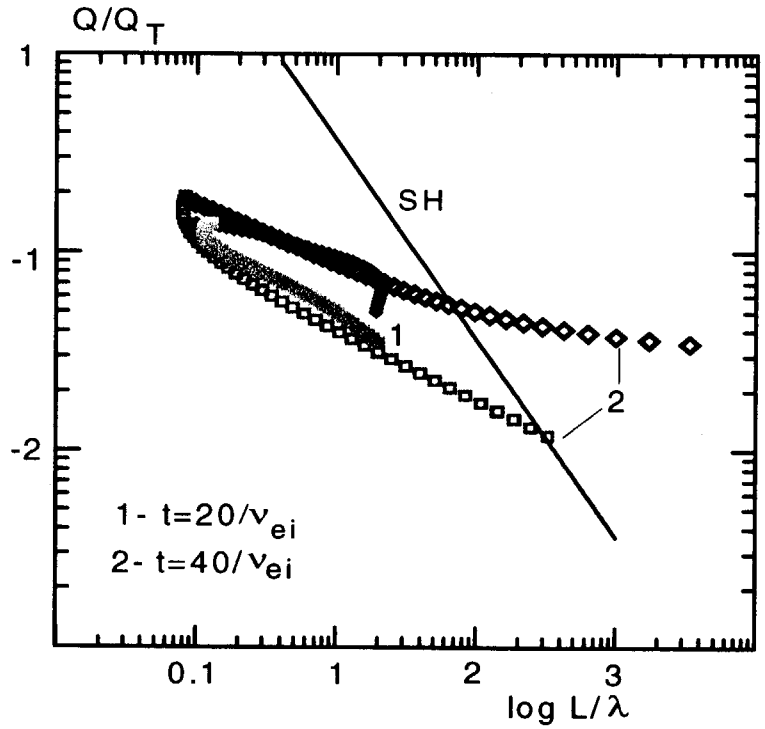

Fig.6a The normalized heat flow versus inverse temperature gradient. The line is the Spitzer-Harm heat flow. All values are defined locally. λ is the local mean free path of an electron. $Q_T=NT_e(T_e/m_e)^{1/2}$.

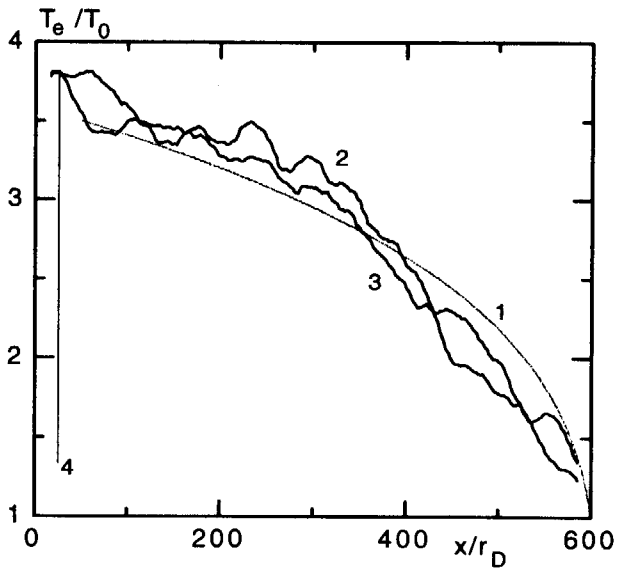

Fig.6b The temporal evolution of the temperature distribution. 1- the steady state temperature distribution, $T(x)/T_0=[(T_l/T_0)^{7/2}(1-x/L)+ x/L]^{2/7}$; 2-$t=300/\omega_{pl}$, 3-$t=500/\omega_{pl}$, 4- the boundary of the "heated" region.

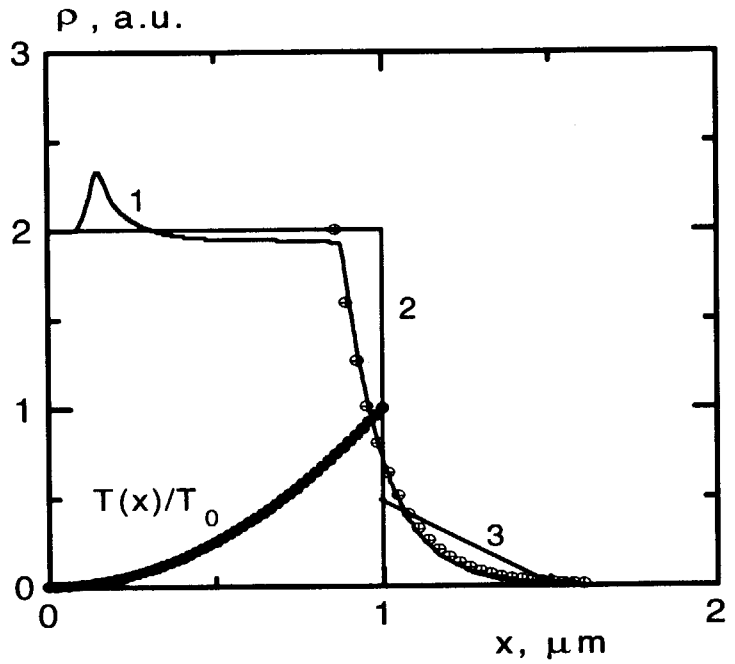

Fig.7 The plasma density profiles are used for the simulation. (1) - the typical density distribution obtained from a hydrodynamic simulation of plasma expansion with the steep distribution of the initial density (2) and the temperature distribution shown by the filled circles. The crosses and the line (3) are the approximations for density distribution Eq.(8a,b)

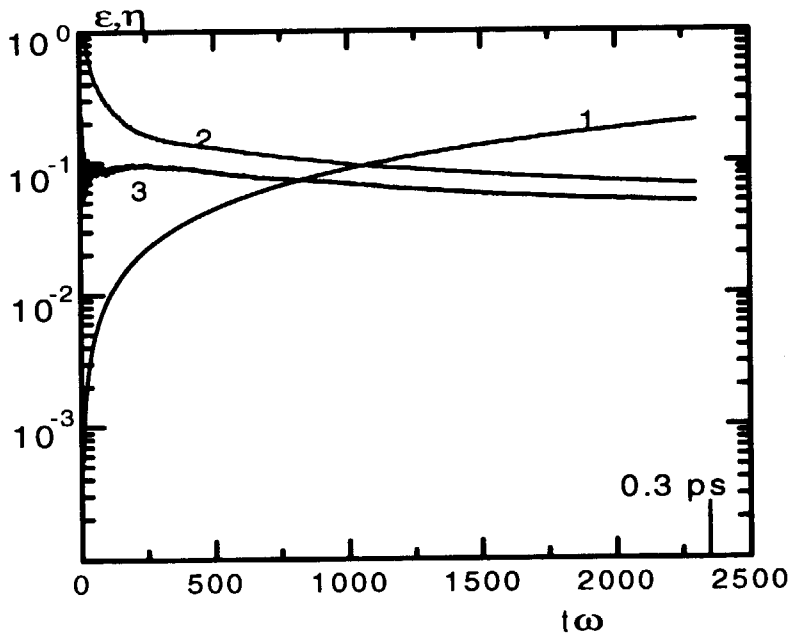

Fig.8 Temporal evolution of the time integrated laser energy (1), the absorption efficiency (2), the portion of energy gone to heat plasma electrons including energy of the electrostatic field (3) for carbon solid density plasma irradiated by KrF laser with the intensity $I=10^{16}$ W/cm^2 and the duration τ=0.3 ps.

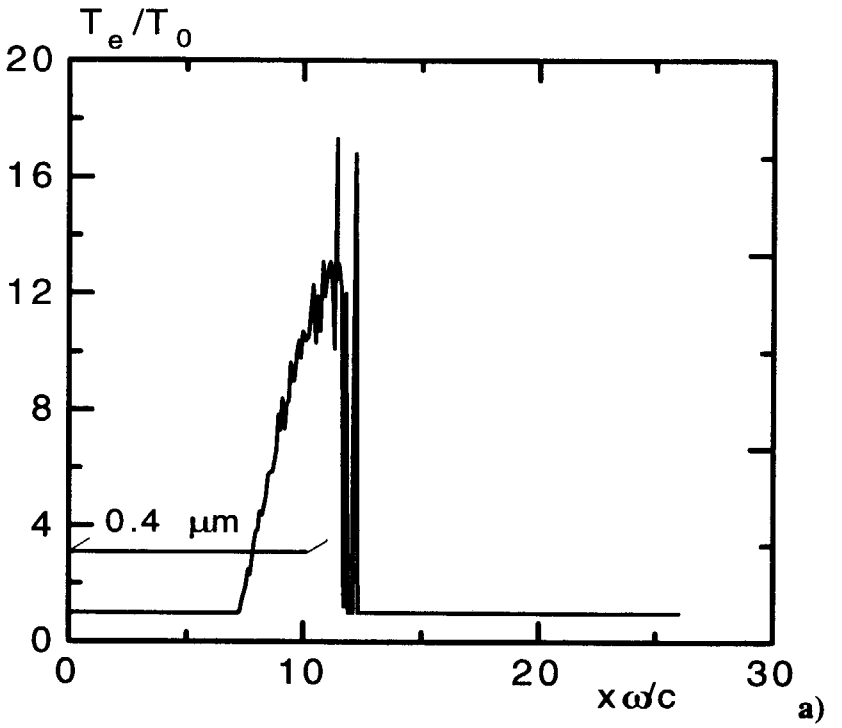
T_e/T_0
20
16
12
8
4
0
0.4 μm
0
10
20
30
xω/c

a)

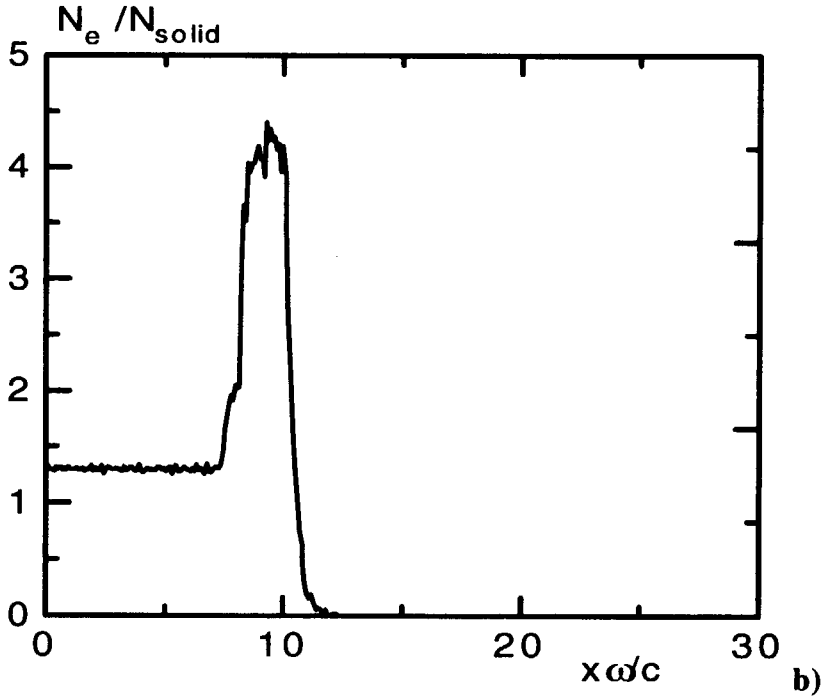
N_e/N_{solid}
5
4
3
2
1
0
0
10
20
30
xω/c

b)

Fig.9 a,b

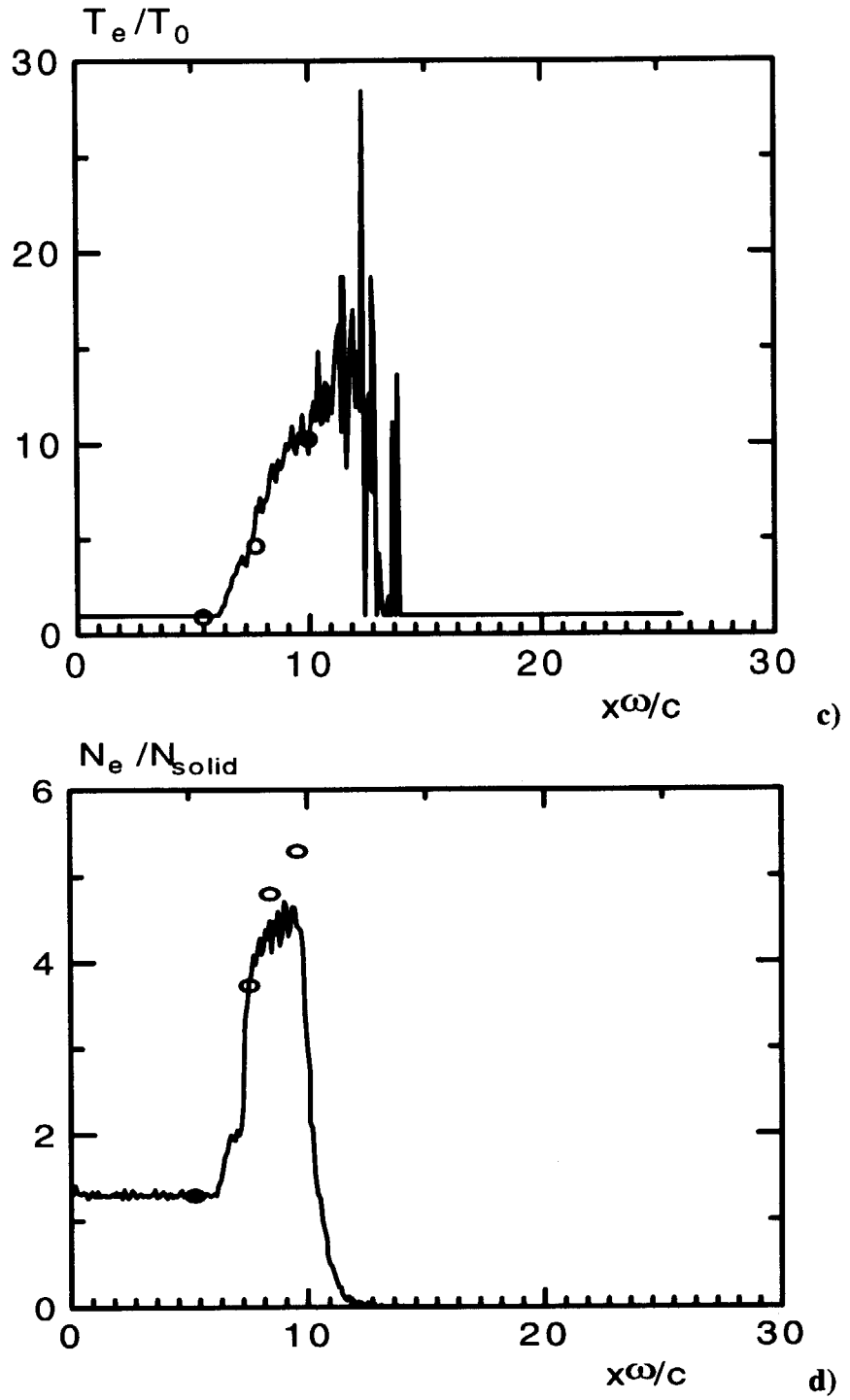

Fig.9 Temporal evolution of the temperature distribution (a,c) and the electron density (b,d) in the solid density carbon plasma irradiated by a s-polarized pulse of KrF laser with the intensity of $I=10^{16}$ W/cm^2.The initial temperature T_0=20 eV.a,b) τ=1500, c,d) τ=2300 (0.3 ps). The circles in Fig.3b, d represent the results of the direct Fokker-Plank simulation [15].

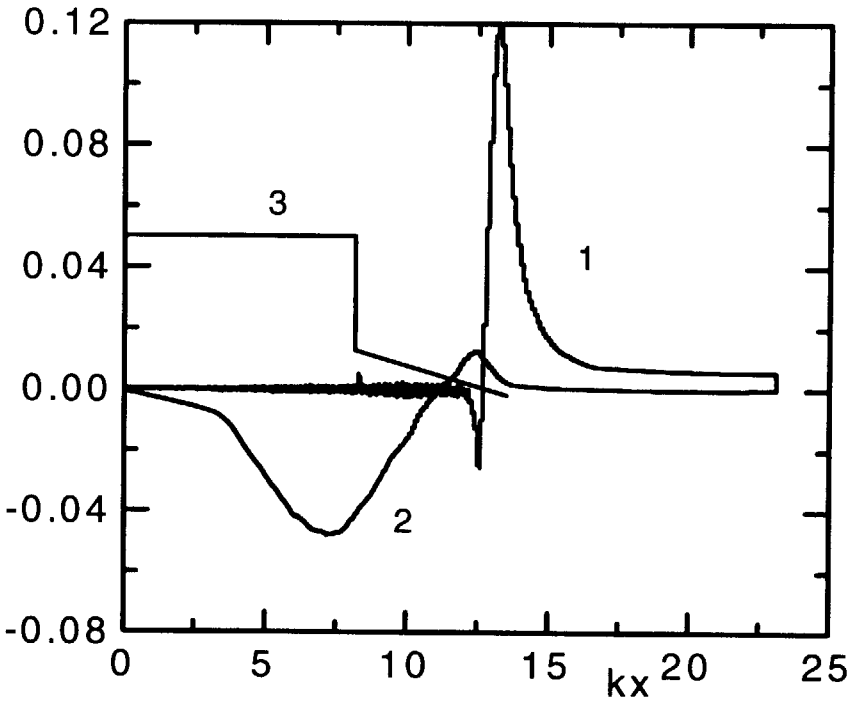

Fig.10 The typical averaged field distributions in the plasma irradiated by a p-polarized pulse laser. (1).-<E_x>, (2).-<H_z>,(3).-the initial plasma density distribution. See, also, [12].

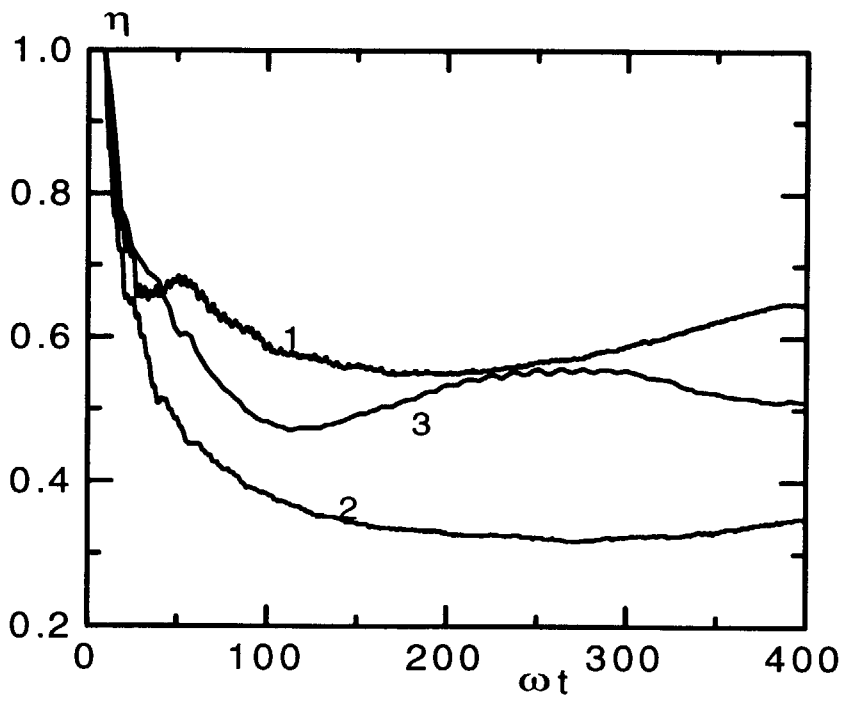

Fig.11 The absorption efficiency of a silicon plasma irradiated by the λ=800 nm, I=4x10^{16} W/cm^2, a p-polarized pulse laser [30] with the prepulse, T_0=10 eV. The oblique incidence at 45^o angle. The linear density profile, (1), (2) - L=0.11 μm, (3)-L=0.22 μm, (1), (3) - N_1= 1.22x10^{22} cm^{-3}, (2) - N_1=2.5x10^{22} cm^{-3}.

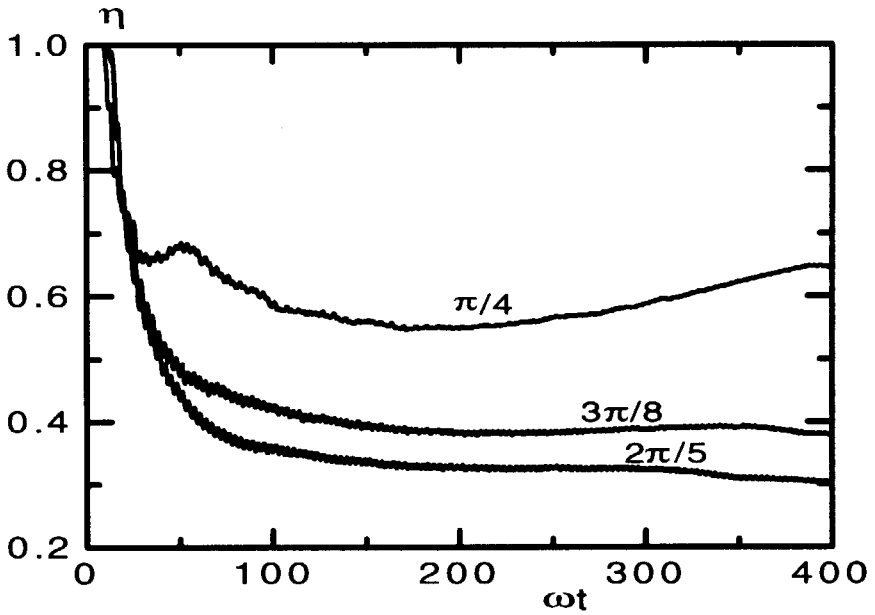

Fig.12 The evolution of the absorption efficiency at different angles of incident for the initial density distribution marked by (1) in Fig.5. The laser pulse parameters are the same.

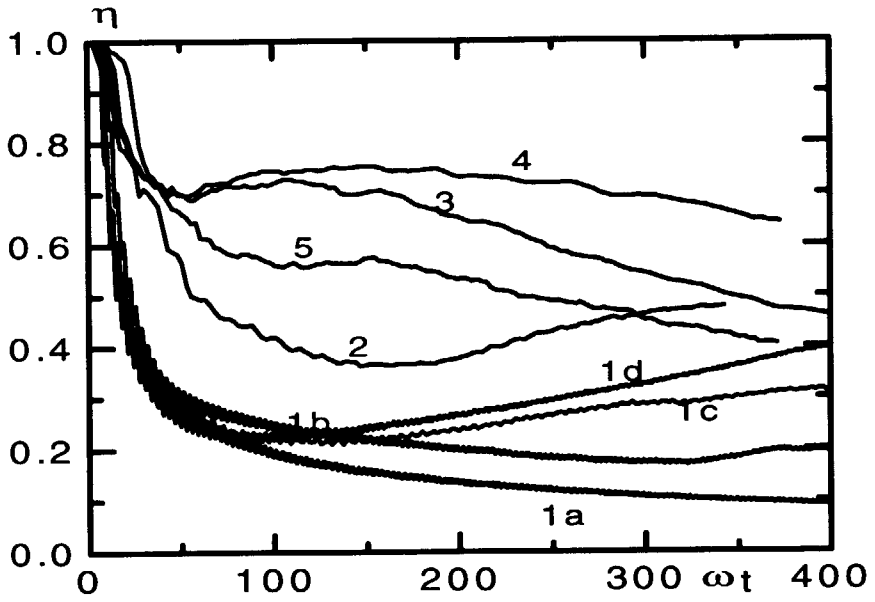

Fig.13 The absorption efficiency of a silicon plasma irradiated by λ=800 nm, I=4x10^{16} W/cm^2((1d)-I=4x10^{17} W/cm^2), a p-polarized pulse laser [30] with the prepulse, T_0=10 eV. The exponential profile. The curves (1b-d), (2), (3), (4), (5) present the absorption of the oblique incidence pulse at 45^o angle. (1) L=0 ,(2) - L=0.11 μm, (3)-L=0.22 μm, (3)-L=0.17 μm, (4)-L=0.41 μm. The curve (1a) is the s-polarized pulse absorption for very steep density gradient. The curve (1c),(1d) is the p-polarized pulse absorption with ion motion included.

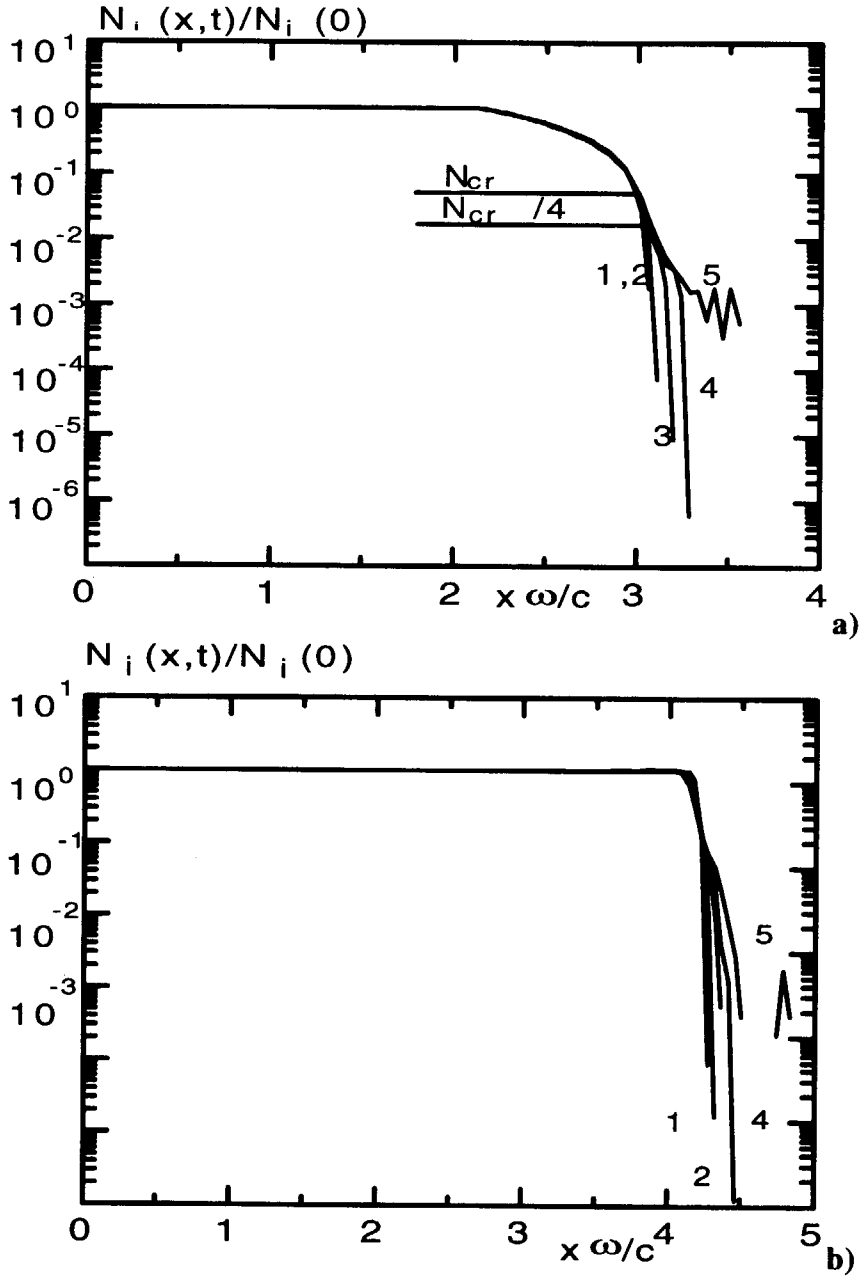

Fig.14 The typical evolution of the ion density during laser pulse 1)$\tau=t\omega=20$, 2)$\tau=150$, 3)$\tau=250$, 4)$\tau=300$, 5)$\tau=400$. (a) the density gradient $L/\lambda=0.22$ and (b) the very steep density gradient.

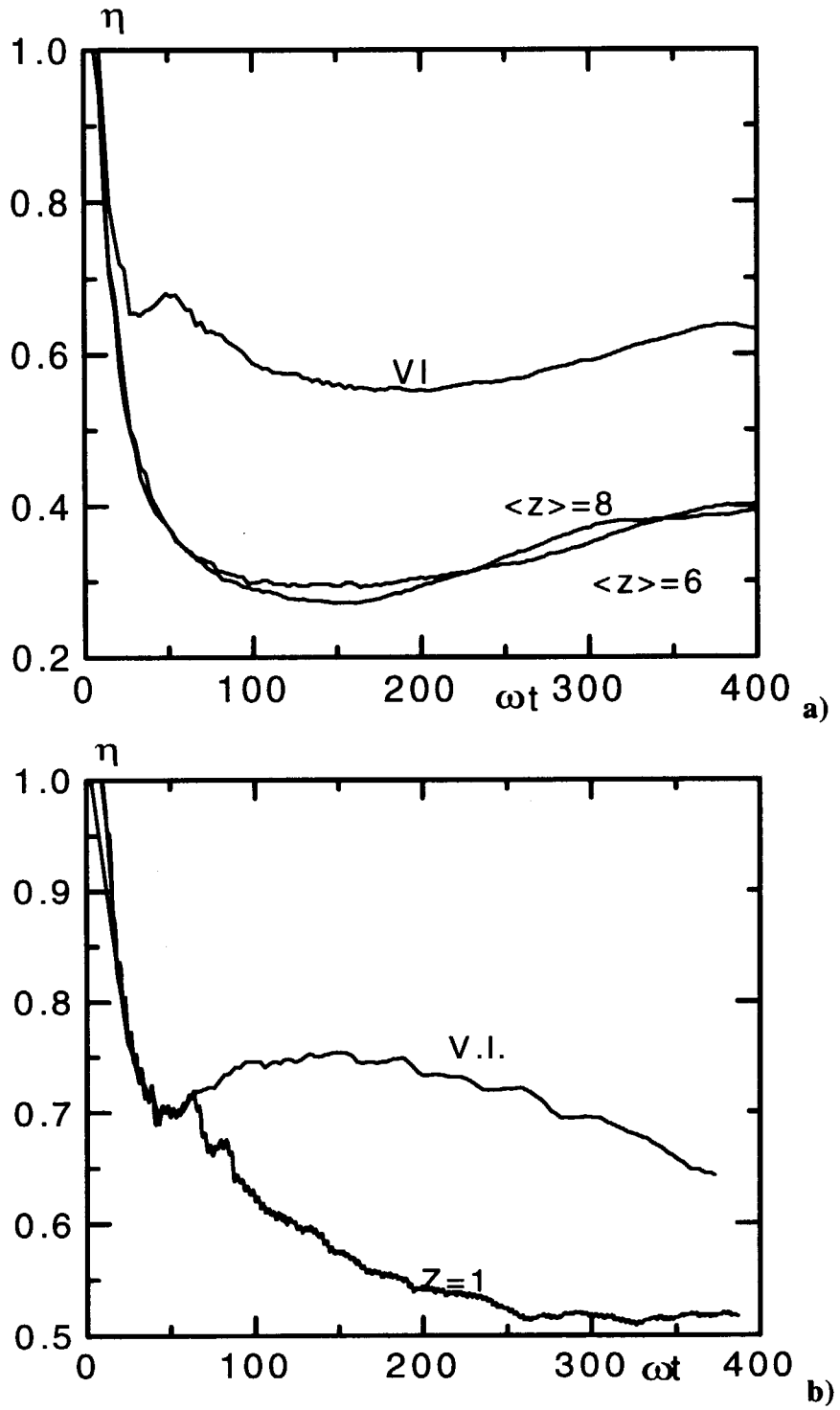

Fig.15 The comparison of the absorption efficiency evolution for the plasma with a fixed ion charge and for the plasma with variable ionization at the linear density approximation (a) and at the exponential density approximation (b). The plasma parameters are optimal for the resonance absorption in the case of the variable ionization.

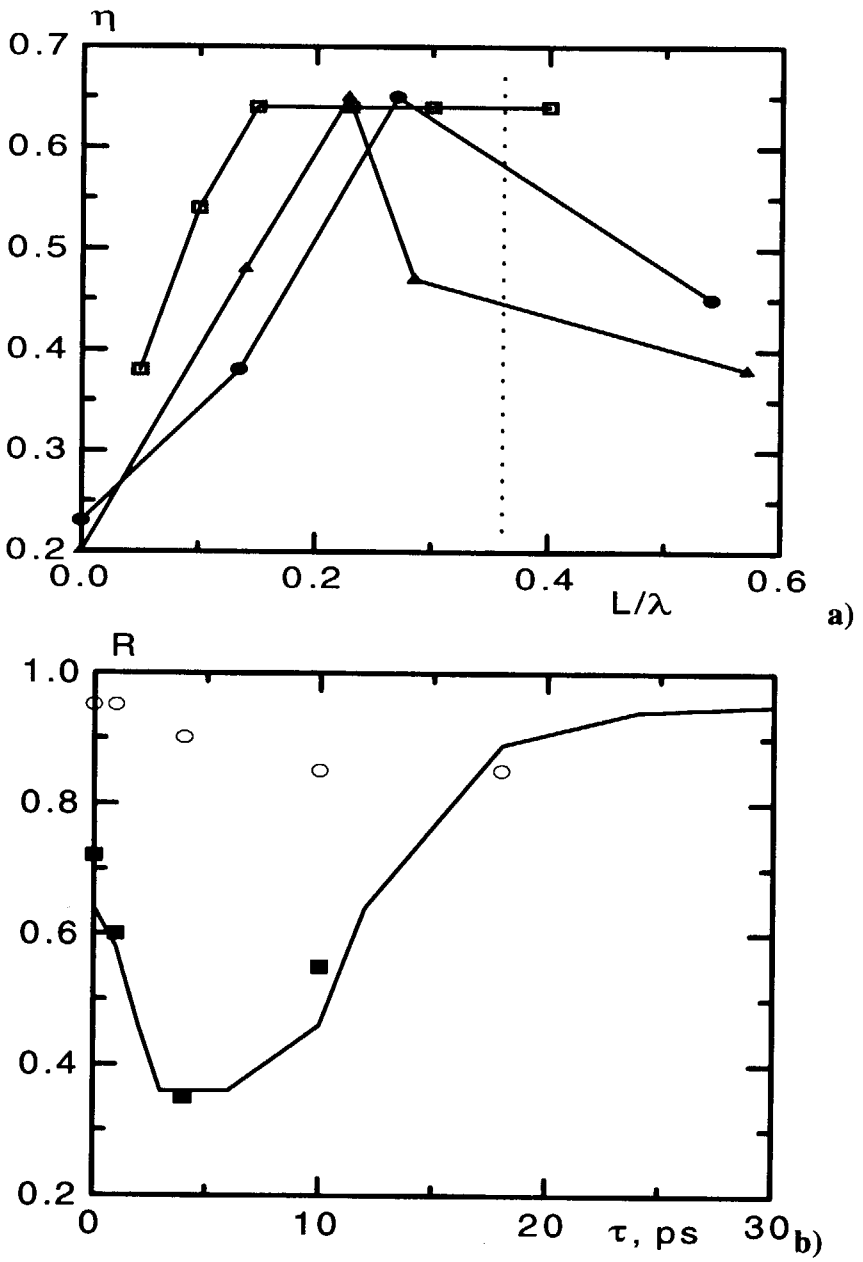

Fig.16 The comparison the results of the measurements (solid curve)[30] and the present calculations for the reflectivity of a silicon plasma. (a)- the dependence of the efficiency on the initial density gradient in the vicinity of the critical density. Filled circles -the linear profile, triangles- the exponential profile, squares- results of [30]. The vertical line represents the maximal measured density gradient [30]. (b) -the dependence of the efficiency on the prepulse delay τ. The open curves is the reflectivity for s-polarized pulse. The squares represent the reflectivity calculated for the p-polarized pulse (45^{o}) for the linear density profile.

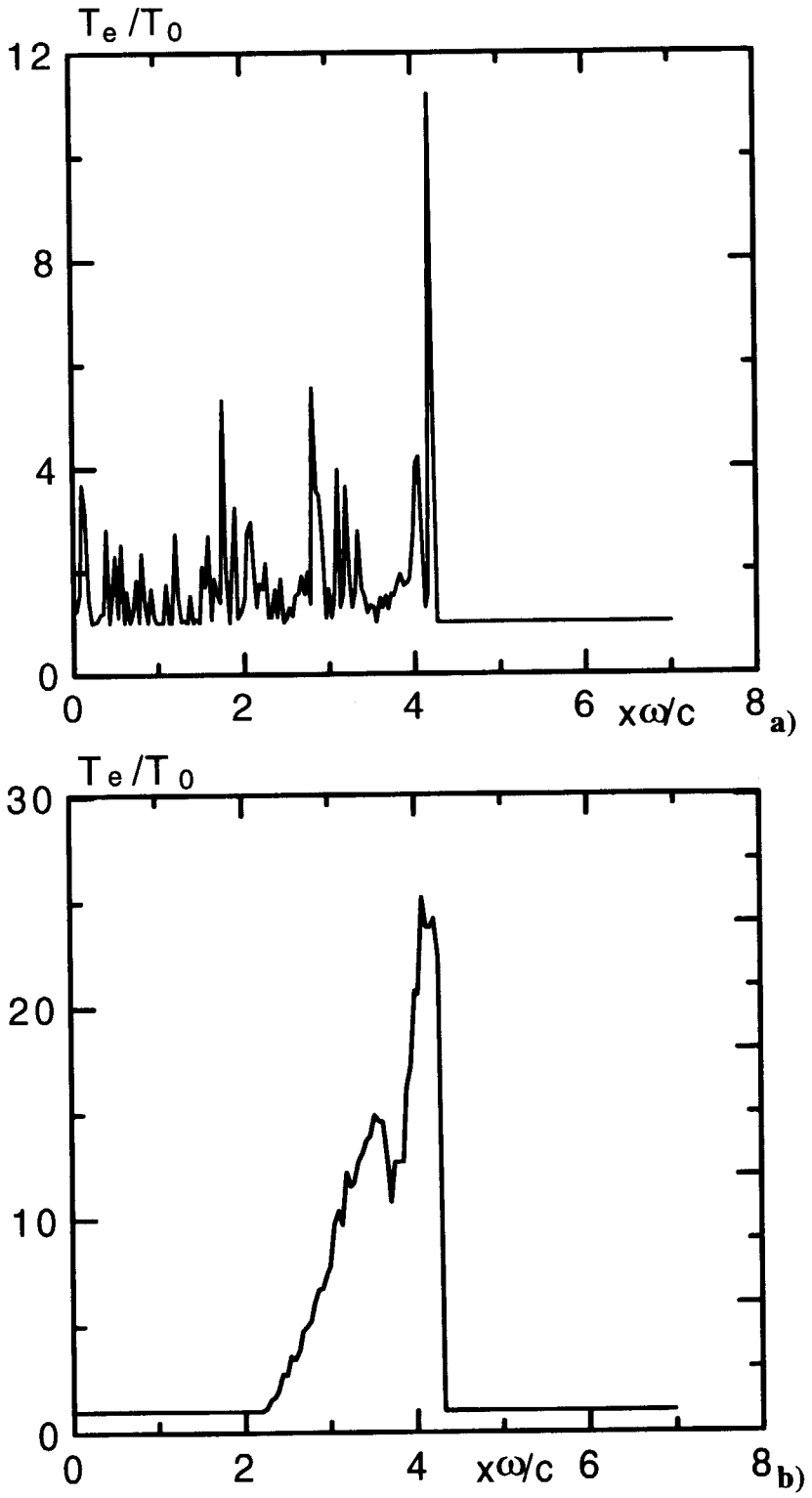

Fig.17 a,b

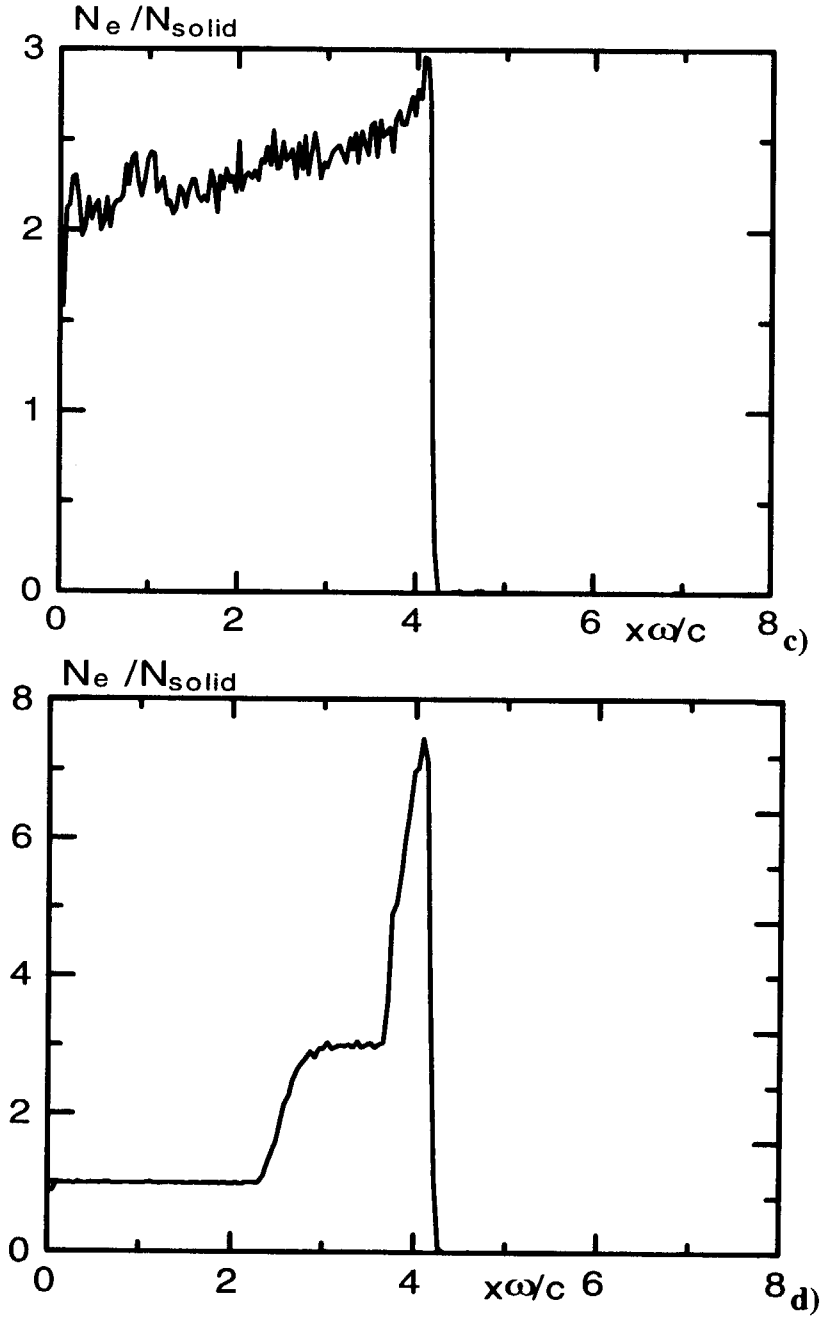

Fig.17 The electron temperature (a,b) and density (c,d) distributions in the silicon plasma irradiated by λ=800 nm, I=4x10^{16} W/cm^2 ,p-polarized pulse laser [30] with very steep density distribution.T_0=10 eV, $\tau=\omega t$=200. (a,c) -no collisions included, (b,d) -e-i and e-e collisions included.

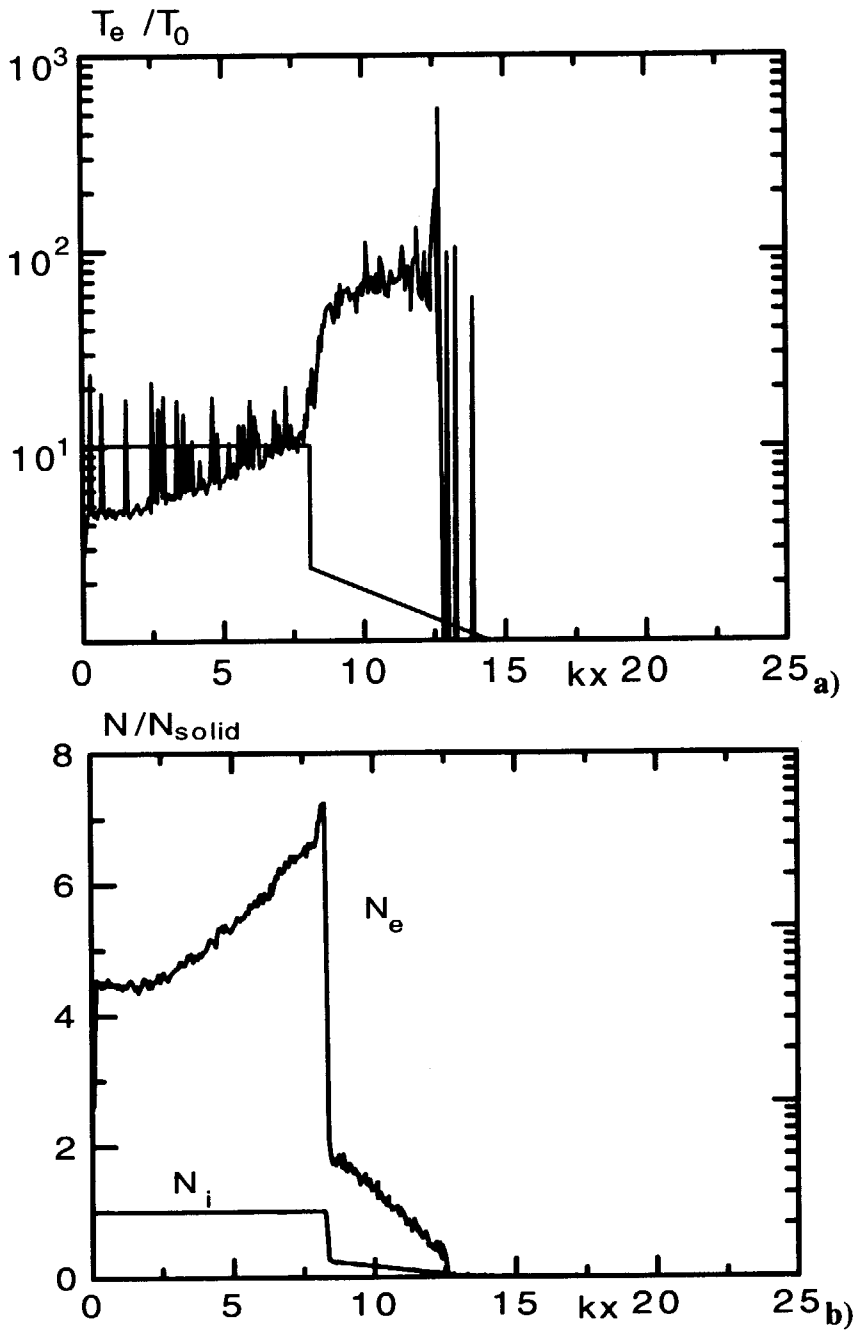

Fig.18 The typical electron temperature (a) and density (b) distributions in a silicon plasma irradiated by λ=800 nm, I=4x10^{16} W/cm^2 ,p-polarized pulse laser [30] with density distribution determined by Eq.(8a) for L/λ=0.22 (4-6 ps prepulse delay) .T_0=10 eV, t=140 fs, k=ω/c. Only electron-ion collisions are included.

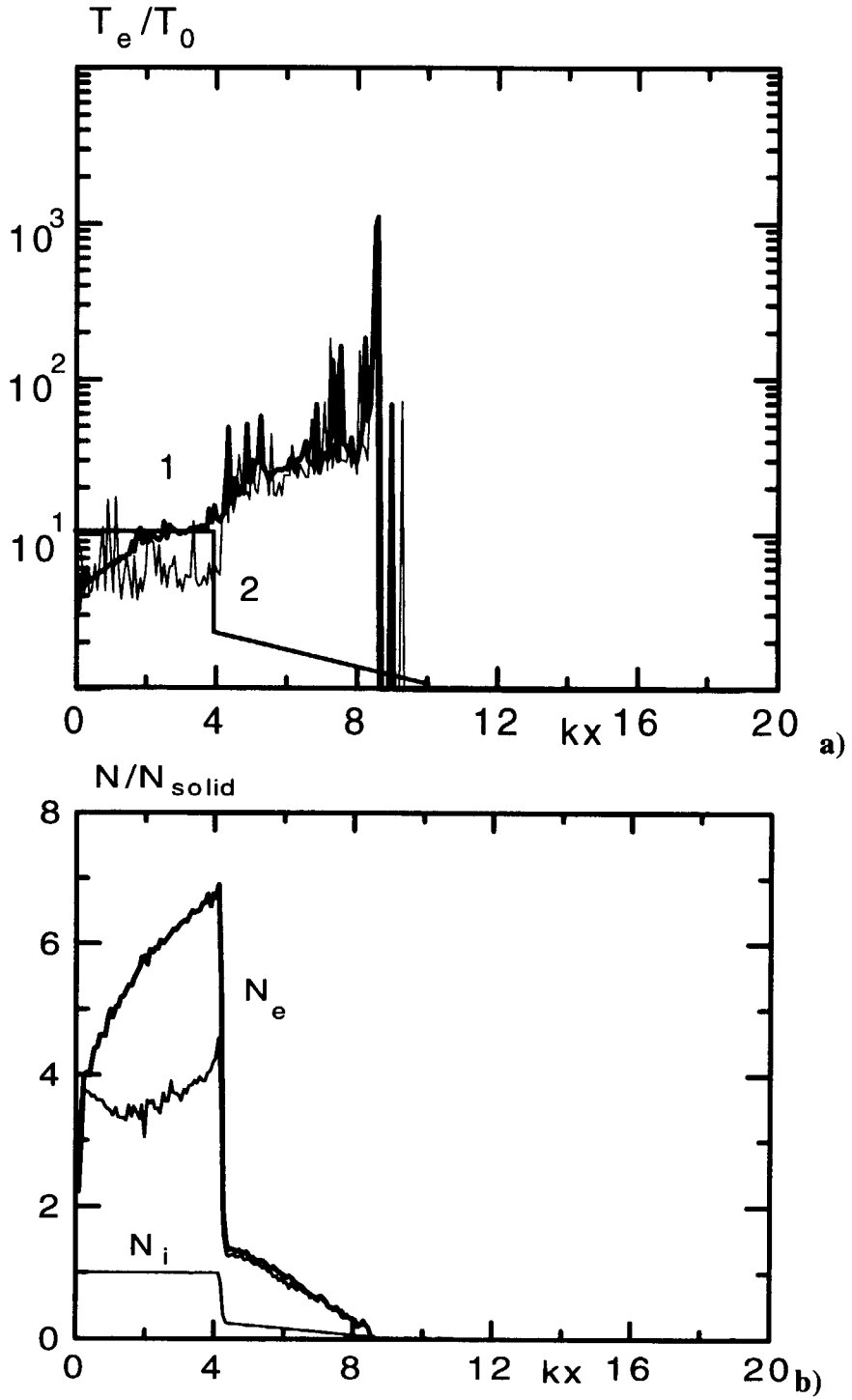

Fig.19 The comparison the results of the simulation the electron temperature (a) and density (b) distributions in a silicon plasma irradiated by λ=800 nm, I=4x10^{16} W/cm^2 , p-polarized pulse laser [30] with the linear density distribution, for L/λ=0.22 (4-6 ps prepulse delay) .T_0=10 eV, t=140 fs, k=ω/c. Solid curves represent the results obtained with the electron-electron collisions, the dashed- without.

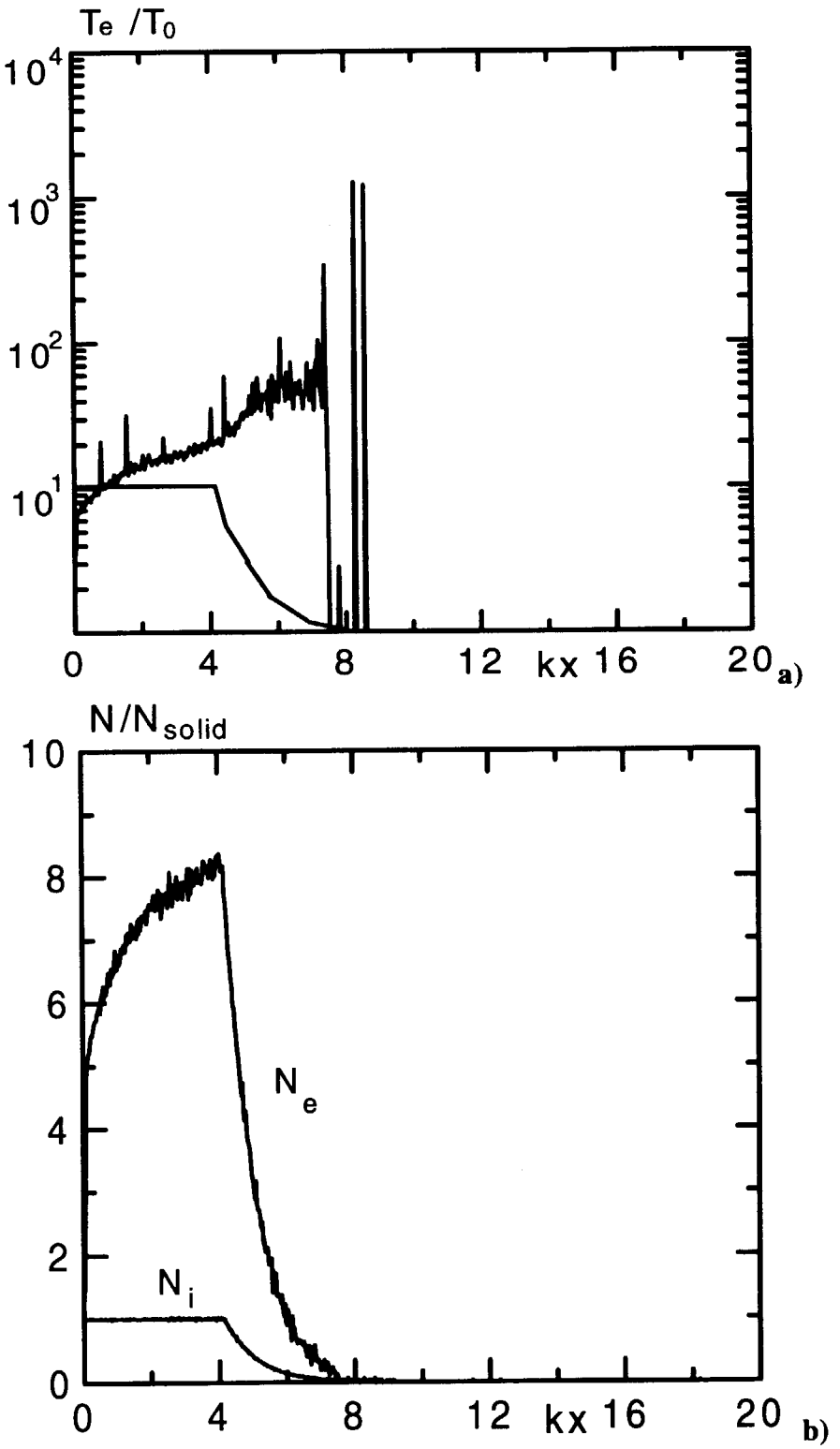

Fig.20 The electron temperature (a) and density (b) distributions in the silicon plasma irradiated by λ=800 nm, I=4x10^{16} W/cm^2 ,p-polarized pulse laser [30] with the exponential density distribution for, L/λ=0.17 (4-6 ps prepulse delay) .T_0=10 eV, t=140 fs, k=ω/c.

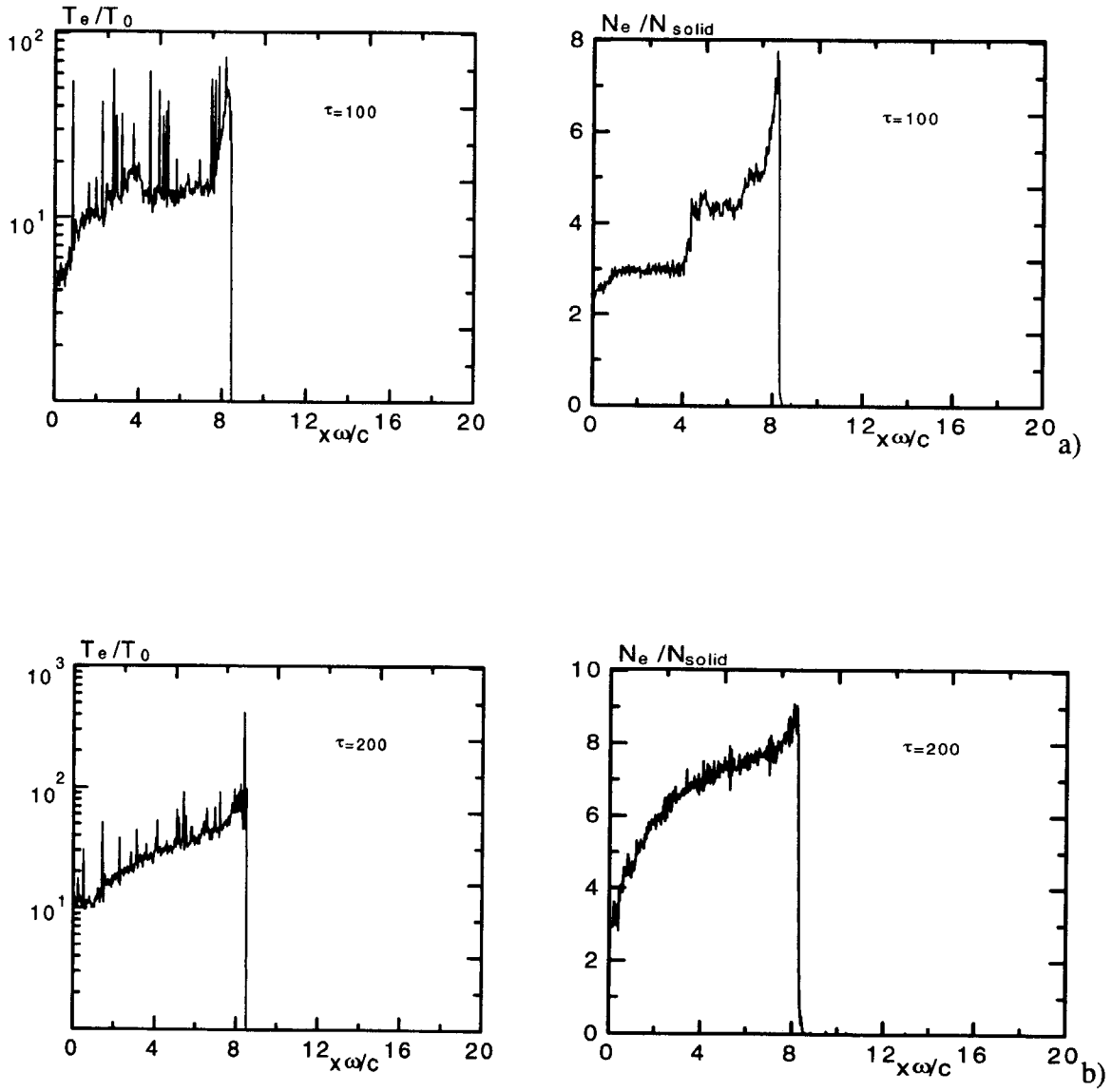
Te /T0
10^2
10^1
τ=100
0
4
8
12
xω/c
16
20
Ne /Nsolid
8
6
4
2
0
τ=100
a)
Te /T0
10^3
10^2
10^1
τ=200
Ne /Nsolid
10
8
6
4
2
0
τ=200
b)

Fig.21a,b

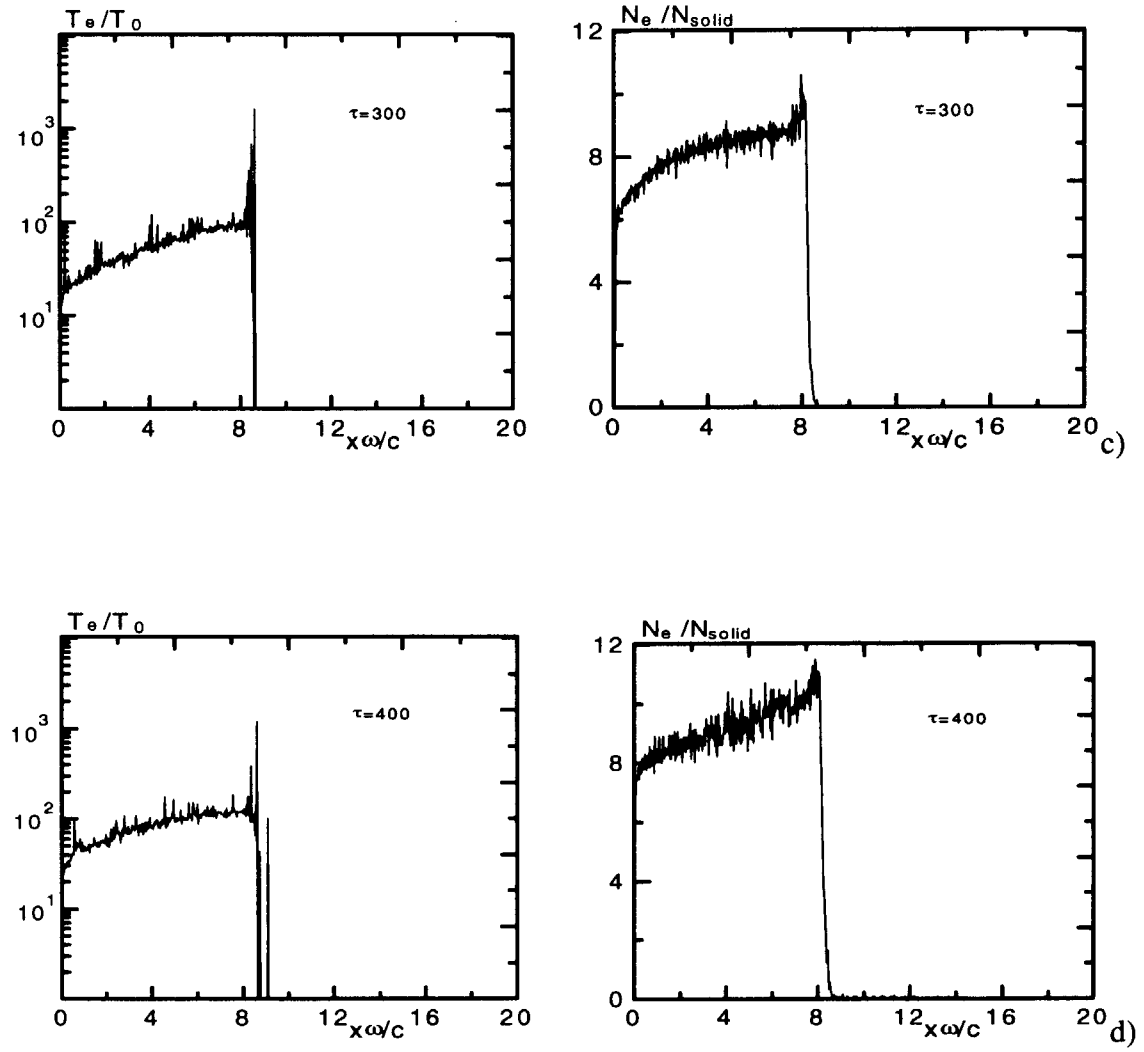

Fig.21 The temporal evolution of the plasma temperature and the electron density in a solid density silicon plasma with the steep density gradient irradiated by a laser pulse with the intensity $I=4\times10^{17}$ Wcm^{-2} and λ=800 nm. a) t=100ω, b) t=200ω, c) t=300ω, d) t=400ω (248ω=100 fs).

国際単位系 (SI) と換算表

表 1　SI基本単位および補助単位

量	名称	記号
長さ	メートル	m
質量	キログラム	kg
時間	秒	s
電流	アンペア	A
熱力学温度	ケルビン	K
物質量	モル	mol
光度	カンデラ	cd
平面角	ラジアン	rad
立体角	ステラジアン	sr

表 2　SIと併用される単位

名称	記号
分，時，日	min，h，d
度，分，秒	°，′，″
リットル	l，L
トン	t
電子ボルト	eV
原子質量単位	u

1 eV = 1.60218 × 10^{-19} J

1 u = 1.66054 × 10^{-27} kg

表 5　SI接頭語

倍数	接頭語	記号
10^{18}	エクサ	E
10^{15}	ペタ	P
10^{12}	テラ	T
10^{9}	ギガ	G
10^{6}	メガ	M
10^{3}	キロ	k
10^{2}	ヘクト	h
10^{1}	デカ	da
10^{-1}	デシ	d
10^{-2}	センチ	c
10^{-3}	ミリ	m
10^{-6}	マイクロ	μ
10^{-9}	ナノ	n
10^{-12}	ピコ	p
10^{-15}	フェムト	f
10^{-18}	アト	a

表 3　固有の名称をもつSI組立単位

量	名称	記号	他のSI単位による表現
周波数	ヘルツ	Hz	s^{-1}
力	ニュートン	N	m·kg/s^2
圧力，応力	パスカル	Pa	N/m^2
エネルギー，仕事，熱量	ジュール	J	N·m
工率，放射束	ワット	W	J/s
電気量，電荷	クーロン	C	A·s
電位，電圧，起電力	ボルト	V	W/A
静電容量	ファラド	F	C/V
電気抵抗	オーム	Ω	V/A
コンダクタンス	ジーメンス	S	A/V
磁束	ウェーバ	Wb	V·s
磁束密度	テスラ	T	Wb/m^2
インダクタンス	ヘンリー	H	Wb/A
セルシウス温度	セルシウス度	℃	
光束	ルーメン	lm	cd·sr
照度	ルクス	lx	lm/m^2
放射能	ベクレル	Bq	s^{-1}
吸収線量	グレイ	Gy	J/kg
線量当量	シーベルト	Sv	J/kg

表 4　SIと共に暫定的に維持される単位

名称	記号
オングストローム	Å
バーン	b
バール	bar
ガル	Gal
キュリー	Ci
レントゲン	R
ラド	rad
レム	rem

1 Å = 0.1 nm = 10^{-10} m

1 b = 100 fm^2 = 10^{-28} m^2

1 bar = 0.1 MPa = 10^5 Pa

1 Gal = 1 cm/s^2 = 10^{-2} m/s^2

1 Ci = 3.7 × 10^{10} Bq

1 R = 2.58 × 10^{-4} C/kg

1 rad = 1 cGy = 10^{-2} Gy

1 rem = 1 cSv = 10^{-2} Sv

（注）

1. 表1－5は「国際単位系」第5版，国際度量衡局 1985年刊行による。ただし，1 eVおよび1 uの値はCODATAの1986年推奨値によった。
2. 表4には海里，ノット，アール，ヘクタールも含まれているが日常の単位なのでここでは省略した。
3. barは，JISでは流体の圧力を表わす場合に限り表2のカテゴリーに分類されている。
4. EC閣僚理事会指令ではbar，barnおよび「血圧の単位」mmHgを表2のカテゴリーに入れている。

換算表

力	N(=10^5 dyn)	kgf	lbf
	1	0.101972	0.224809
	9.80665	1	2.20462
	4.44822	0.453592	1

粘度　1 Pa·s(N·s/m^2) = 10 P(ポアズ)(g/(cm·s))

動粘度　1 m^2/s = 10^4 St(ストークス)(cm^2/s)

圧力	MPa(=10 bar)	kgf/cm^2	atm	mmHg(Torr)	lbf/in^2(psi)
	1	10.1972	9.86923	7.50062 × 10^3	145.038
	0.0980665	1	0.967841	735.559	14.2233
	0.101325	1.03323	1	760	14.6959
	1.33322 × 10^{-4}	1.35951 × 10^{-3}	1.31579 × 10^{-3}	1	1.93368 × 10^{-2}
	6.89476 × 10^{-3}	7.03070 × 10^{-2}	6.80460 × 10^{-2}	51.7149	1

エネルギー・仕事・熱量	J(=10^7 erg)	kgf·m	kW·h	cal(計量法)	Btu	ft·lbf	eV
	1	0.101972	2.77778 × 10^{-7}	0.238889	9.47813 × 10^{-4}	0.737562	6.24150 × 10^{18}
	9.80665	1	2.72407 × 10^{-6}	2.34270	9.29487 × 10^{-3}	7.23301	6.12082 × 10^{19}
	3.6 × 10^6	3.67098 × 10^5	1	8.59999 × 10^5	3412.13	2.65522 × 10^6	2.24694 × 10^{25}
	4.18605	0.426858	1.16279 × 10^{-6}	1	3.96759 × 10^{-3}	3.08747	2.61272 × 10^{19}
	1055.06	107.586	2.93072 × 10^{-4}	252.042	1	778.172	6.58515 × 10^{21}
	1.35582	0.138255	3.76616 × 10^{-7}	0.323890	1.28506 × 10^{-3}	1	8.46233 × 10^{18}
	1.60218 × 10^{-19}	1.63377 × 10^{-20}	4.45050 × 10^{-26}	3.82743 × 10^{-20}	1.51857 × 10^{-22}	1.18171 × 10^{-19}	1

1 cal = 4.18605 J (計量法)
= 4.184 J (熱化学)
= 4.1855 J (15 °C)
= 4.1868 J (国際蒸気表)

仕事率　1 PS (仏馬力)
= 75 kgf·m/s
= 735.499 W

放射能	Bq	Ci
	1	2.70270 × 10^{-11}
	3.7 × 10^{10}	1

吸収線量	Gy	rad
	1	100
	0.01	1

照射線量	C/kg	R
	1	3876
	2.58 × 10^{-4}	1

線量当量	Sv	rem
	1	100
	0.01	1

（86年12月26日現在）

HYBRID PARTICLE-IN-CELL(PIC)SIMULATION OF HEAT TRANSFER AND IONIZATION BALANCE IN OVERDENSE PLASMAS IRRADIATED BY SUBPICOSECOND PULSE LASERS